Accepted Manuscript

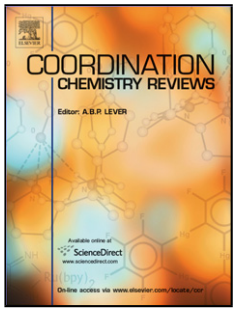

Title: High-energy metal-organic frameworks (HE-MOFs): Synthesis, Structure and Energetic Performance

Author: Sheng Zhang Qi Yang Xiangyu Liu Xiaoni Qu Qing Wei Gang Xie Sanping Chen Shengli Gao

PII: S0010-8545(15)00276-3
DOI: http://dx.doi.org/doi:10.1016/j.ccr.2015.08.006
Reference: CCR 112128

To appear in: *Coordination Chemistry Reviews*

Received date: 22-7-2015
Revised date: 20-8-2015
Accepted date: 20-8-2015

Please cite this article as: S. Zhang, Q. Yang, X. Liu, X. Qu, Q. Wei, G. Xie, S. Chen, S. Gao, High-energy metal-organic frameworks (HE-MOFs): Synthesis, Structure and Energetic Performance, *Coordination Chemistry Reviews* (2015), http://dx.doi.org/10.1016/j.ccr.2015.08.006

This is a PDF file of an unedited manuscript that has been accepted for publication. As a service to our customers we are providing this early version of the manuscript. The manuscript will undergo copyediting, typesetting, and review of the resulting proof before it is published in its final form. Please note that during the production process errors may be discovered which could affect the content, and all legal disclaimers that apply to the journal pertain.

Graphical Abstract (for review)

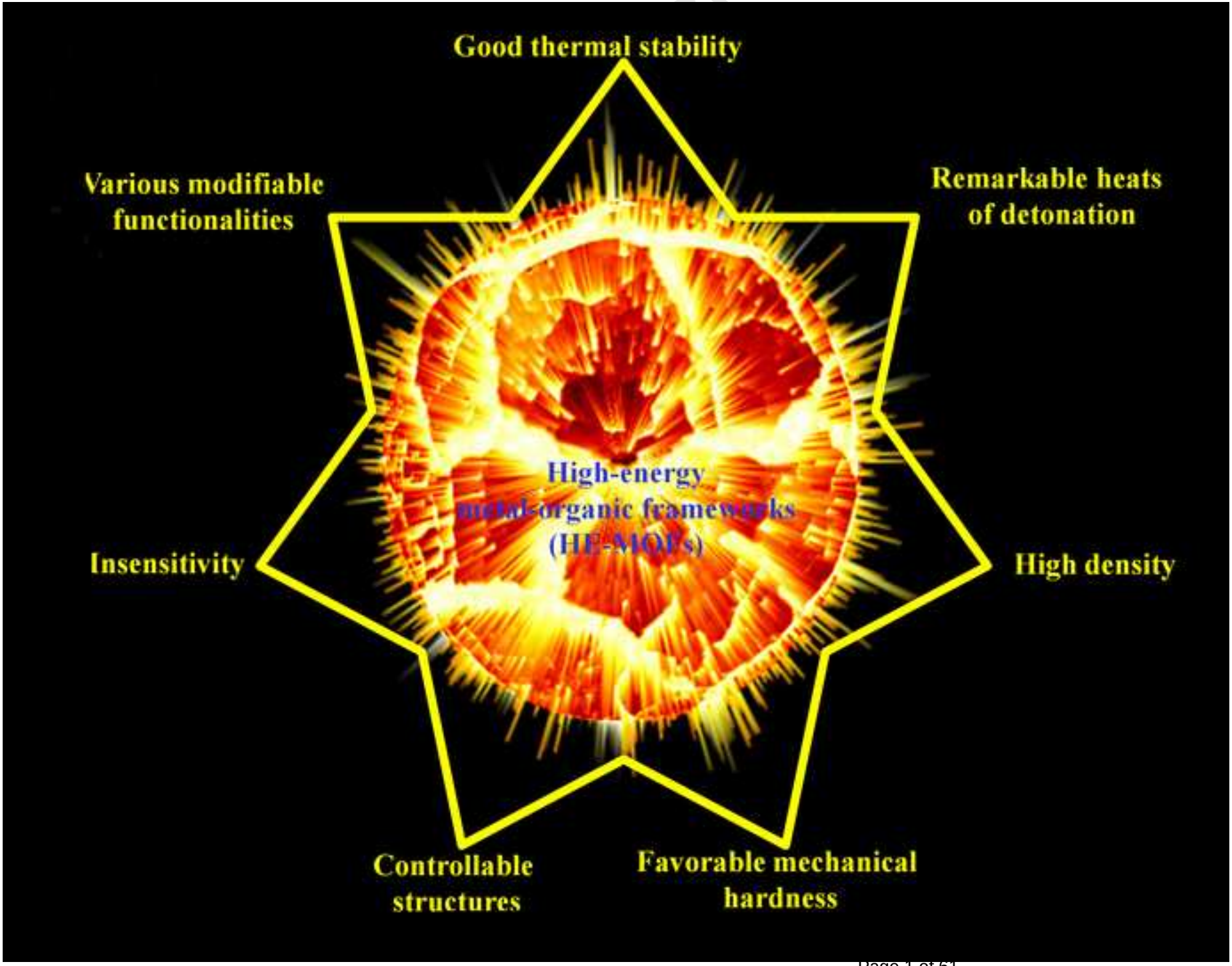

ACCEPTED MANUSCRIPT

Highlights

- Based on various nitrogen-rich energetic ligands, high-energy metal-organic frameworks (HE-MOFs) have attracted considerable attention in the field of energetic materials owing to controllable structures, various modifiable functionalities, high density, remarkable heats of detonation, insensitivity, good thermal stability and favorable mechanical hardness.
- The purpose of this review is to provide readers with an inductive overview of both in-depth understanding of energetic-sensitive-structural correlations and the development and outlook in the field of high-energy-density materials (HEDMs), which is favorable to guide the future design of novel HEDMs through the combination of experiment and theory.

Accepted Manuscript

ACCEPTED MANUSCRIPT

High-energy metal-organic frameworks (HE-MOFs): Synthesis, Structure and Energetic Performance

Sheng Zhang,[a] Qi Yang, [a] Xiangyu Liu, [a,b] Xiaoni Qu, [a] Qing Wei, [a] Gang Xie, [a] Sanping Chen, [*a] Shengli Gao [a]

[a] *Key Laboratory of Synthetic and Natural Functional Molecule Chemistry of Ministry of Education, College of Chemistry and Materials Science, Northwest University, Xi'an, Shaanxi 710069, China*

[b] *School of Chemistry and Chemical Engineering, Ningxia University, Yinchuan 750021, China*

Corresponding author

Dr. Sanping Chen

E-mail address: sanpingchen@126.com

Accepted Manuscript

ACCEPTED MANUSCRIPT

Abstract

Recent progress in high-energy metal-organic frameworks (HE-MOFs), not only a burgeoning branch of growing interest in energetic materials but also a particular class of metal-organic frameworks (MOFs), is covered in this review. HE-MOFs, based on various nitrogen-rich energetic ligands, may serve as an effective approach for systematically studying the energetic-sensitive-structural relationships and guiding the future design of new generation high-energy-density materials (HEDMs) because of their various advantages, including controllable structures, various modifiable functionalities, high density, remarkable heats of detonation, insensitivity, good thermal stability and favorable mechanical hardness. In the review, an inductive overview of the development and outlook in the field of HEDMs, particularly those with one-, two- and three-dimensional (1D-3D) architectures, are presented.

Accepted Manuscript

ACCEPTED MANUSCRIPT

***Abbreviations**:* MOFs, metal-organic frameworks; HE-MOFs, high-energy metal-organic frameworks; HEDMs, high-energy-density materials; DATr, 3,5-diamine-1*H*-1,2,4-triazole; HATr, 3-hydrazino-4-amino-1,2,4-triazole; H_2tztr, 3-(tetrazol-5-yl)triazole; ATZ, 4-amino-1,2,4-triazole; Mtta, 5-methyl tetrazole; AzTTO, 5-(5-azido-1*H*-1,2,4-triazol-3-yl)-1*H*-tetrazol-1-ol; ANBT, 5-(5-amine-1*H*-1,2,4-triazol-3-yl)-3-nitro-1*H*-1,2,4-triazole; NTTO, 5-(5-nitro-1*H*-1,2,4-triazol-3-yl)-1*H*-tetrazol-1-ol; DABT, 3,3'-diamino-5,5'-bis(1*H*-1,2,4-triazole); AzNBT, 5-(5-azido-1*H*-1,2,4-triazol-3-yl)-3-nitro-1*H*-1,2,4-triazole; DNBT, 3,3'-dinitro-5,5'-bis(1*H*-1,2,4-triazole); NNBT, 5-(5-nitrimino-1,3*H*-1,2,4-triazol-3-yl)-3-nitro-1*H*-1,2,4-triazole; BTE, 1,2-Bis(1,2,4-triazole-1-yl)ethane; Atrz, 4,4'-azo-1,2,4-triazole; 5-AT, 5-amino-1*H*-tetrazole; H_2TZA, Tetrazole-1-acetic; DAT, 1,5-diaminotetrazole (1,5-diamino-*1H*-tetrazole); H_2AtNO_2, 5-nitriminotetrazole; H_2tzeg, *N*-[2-(1H-tetrazol-5-yl)ethyl]glycine; H_2BT, 5,5'-bis(tetrazolate); H_2BTA, *N*,*N*-bis(1*H*-tetrazol-5-yl)-amine; H_2BTE, 1,2-bis(tetrazol-5-yl)ethane; ABTr, 5,5'-azobistetrazole; H_2OBT, 5,5'-(1,2-phenylene)bis(1*H*-tetrazole); H_2BTB, 5,5'-(1,3-phenylene)bis(1*H*-tetrazole); H_2BDT, 5,5'-(1,4-phenylene)bis(1*H*-tetrazole); MHT, 5-(1-methylhydrazinyl)tetrazole; ANPZ, 2,6-diamino-3,5-dinitropyrazine; TMMAP, 2,4,6-triazido-5-(azidomethyl)pyrimidine; TAT, 2,4,6-triazido-1,3,5-triazine; DiAT, 3,6-diazido-1,2,4,5-tetrazine; NADAT, 4,6-diazido-*N*-nitro-1,3,5-triazin-2-amine; TAH, 2,5,8-tri(azido)-s-heptazine; DGT-DO, 3,6-diguanidino-1,2,4,5-tetrazine-1,4-di-*N*-oxide; TAAT, 1,2-bis(4,6-diazido-1,3,5-triazin-2-yl)diazene; DAAT, 6-((6-amino-1,2,4,5-tetrazin-3-yl)diazenyl)-1,2,4,5-tetrazin-3-amine; DAF, 3,4-diaminofurazan; ANF, 3-amino-4-nitrofurazan; DNF, 3,4-dinitrofurazan; DNBF, 4,4'-dinitro-3,3'-bifurazan; FOF-2, 3,3'-dicyanodifurazanyl ether; FOF-1, 4,4'-dinitrodifurazalylether; DAAzF, 4,4'-diamino-3,3'-azofurazan; DNAzBF, 4,4'-dinitro-3,3'-azo-bis(furazan); H2BTF, 3,4-bis(1*H*-5-tetrazole)furazan; H_2BOTFAZ, Bis(1-hydroxytetrazolyl)furazane; DTZAF, 1,2-bis(4-(tetrazol-5-yl)-1,2,5-oxadiazol-3-yl)diazene; H_2BTFOF, 4,4'-oxybis[3,3'-(1*H*-5-tetrazol)]furazan; TNT, 2,4,6-trinitrotoluene; LA, lead azide; LS, lead styphnate; PETN, pentaerythrite tetranitrate; RDX, 1,3,5-trinitro-1,3,5-triazacyclohexane; HMX, 1,3,5,7-tetranitro-1,3,5,7-tetraazacyclooctane; TATB, triamino trinitrobenzene; PA, picrate acid; en, ethylenediamine; pn, 1,2-diaminopropane; HP, hydrazine perchlorate; AP, ammonium perchlorate; 3,5-DNBA, 3,5-dinitrobenzoic acid; CL-20, hexanitrohexaazaisowurtzitane; FOX-7, 1,1-diamino-2,2-dinitroethylene; HNB, hexanitrobenzene; ONC, octanitrocubane; Tetryl, 2,4,6-trinitrophenylmethylnitramine; MF, mercury fulminate; T_{dec}, decomposition temperature; Ω, oxygen balance; IS, impact sensitivity; FS, friction sensitivity; ESD, electrostatic sensitivity; ρ, the density value from X-ray diffraction; $\Delta_f H_m^\theta$, the standard molar enthalpy of formation; $\Delta_c H_m^\theta$, the standard molar enthalpy of combustion; $\Delta E_{det,}$ the energy of detonation; DFT, density functional theory; $\Delta H_{det,}$ the heat of detonation; D, detonation velocity; P, Detonation pressure.

Accepted Manuscript

ACCEPTED MANUSCRIPT

1. Introduction

Metal-organic frameworks (MOFs) have attracted extensive interest because of their stable architectures, controllable structures, modifiable properties and potential applications in chemical gas storage, chemical separation, heterogeneous catalysis, sensing, conductivity, chiral separation, drug delivery, and so forth [1-5]. Therein, metal ions or clusters are bridged by organic or inorganic ligands into one-, two- and three-dimensional (1D-3D) architectures. Due to the inherent advantages [6], such as high density, favorable thermal stability and excellent mechanical strength and hardness, it is predicted that MOFs would become as potential energetic materials if combined with high energy and enormous heat of detonation, inspiring an attemptable juncture for the advancement of high-energy-density materials (HEDMs).

As known, numerous metal-based explosives, including metal salts and coordination compounds, have been utilized as initiating primary explosives for many decades. A number of them are consisted of metal ions (Pb^{2+} and Ag^{+} etc.), energetic anions (such as N_3^- and NO_3^-) or simple energetic ligands (triazole, tetrazole, tetrazine, hydrazine and so on). In the case of high-energy bridging ligands (e.g., nitrogen-rich or nitro-containing compounds), high-energy MOFs (HE-MOFs) with different dimensionalities (1D, 2D or 3D) could be assembled from the configurations of metal ions and the coordination modes of ligands on the basis of coordination chemistry. From the perspective of the constituents of MOFs, inorganic components would endue them with high density, benign mechanical hardness, good thermal stability, while organic energetic components would endow them with energy sources, diverse structures, topologies and regulation functions. In addition, the structural frameworks and dimensionalities of the target MOFs could be regulated through other factors, such as temperature, solvent effect, pH, templates, stoichiometry and guest molecule [6-8]. In this sense, the concept of designing HE-MOFs would provide a unique architectural platform for developing new-generation HEDMs. During the past three years, HE-MOFs experienced and gained rapid development, which is living up to expectations, involving high density, low sensitivity, favorable thermostability, remarkable detonation performance and heat of detonation due to their strong structural reinforcements and extensive coordination networks [9-24]. In 2014, Zhang and Shreeve highlighted the application prospects and development potentials of HE-MOFs in the field of energetic materials [6]. We are constantly dedicated in pushing progress towards new-generation energetic materials with better

ACCEPTED MANUSCRIPT

performance and mechanical insensitivity in meeting the demands of high energy and safety in recent years [13-17,25,26]. While it is found experimentally that once various nitrogen-rich energetic ligands combine with metal ions, the sensitivity of HE-MOFs grows exponentially as the energy increases, which to a great extent may restrict the applications of HE-MOFs in the field of energetic materials. Sequentially, it is significant to make an inductive report about energetic MOFs which is considered as the potential candidate of HEDMs.

This review article examines the syntheses, structures and properties of HE-MOFs with diverse dimensional networks in nearly a decade, which is not intended to be comprehensive discussion of every known HE-MOFs. The purpose of this article is to provide readers with an overview of in-depth understanding of energetic-sensitive-structural correlations and guide the future design of novel HEDMs through the combination of experiment and theory.

2. High-energy bridging ligands and energetic moieties

So far, the pioneering scientists, such as Klapöke, Shreeve as well as others had constructed considerable research about high-nitrogen energetic salts and compounds on the basis of azide, hydrazine, imidazole, triazole, tetrazole, triazine, tetrazine, furazan (furoxan) and their derivatives [27-49]. Because the average bond energies of C-N, N-N, N=N and N≡N are 273 kJ mol^{-1}, 160 kJ mol^{-1}, 418 kJ mol^{-1} and 954 kJ mol^{-1}, respectively, exhibiting the huge energy potential [50-58].

2.1 Triazole, tetrazole and their derivatives

Scheme 1 Triazole and its derivatives.

Scheme 2 Tetrazole and its derivatives.

Five-membered nitrogen-rich heterocyclic compounds are traditional sources of energetic materials [5]. Many research groups have gained abundant significant findings on the basis of triazole, tetrazole and their derivatives (Schemes 1-2). Being rich in electron pairs, nitrogen-rich energetic ligands can react with some acids resulting in the formation of stable salts or coordinate with metal ions. What's more, azole-based compounds are very outstanding high-energy bridging ligands because the nitrogen atoms in the ring have lone pair electrons and provide necessary

ACCEPTED MANUSCRIPT

conditions to coordinate with the central metal ions. The role of azole ring with potential N-coordination sites could extend structures, resulting in different dimensionalities. The frequently-used nitrogen-rich heterocyclic ligands are as follows:

Amino tetrazoles have high content of nitrogen, such as 5-amino-*1H*-tetrazole (5-AT, N% = 82.33), 1,5-diamino-*1H*-tetrazole (DAT, N% = 83.97), 3-hydrazino-4-amino-1,2,4-triazole (HATr, N% = 73.65%), 4-amino-1,2,4-triazole (ATZ, N% = 66.63%), 5-(1-methylhydrazinyl)tetrazole (MHT, N% = 73.65%). Despite their large positive enthalpies of formation, they exhibit surprisingly high thermal stabilities.

H_2BTA (N,N-bis(1H-tetrazole-5-yl)-amine), is also a good choice to construct HE-MOFs, based on the following reasons: 1) The high nitrogen content (N%=82.34%) could improve the energetic performance of the target compound [59]; 2) The versatile chelating-bridging coordination modes are propitious to construct high-dimensional framework [60]; 3) The nitrogen atoms are predicted to be involved in the hydrogen-bond motifs to capture energetic moieties [61]; 4) The predominant decomposition products are environmentally benign nitrogen gases; 5) The azide group hidden in a aminotetrazole, is known as the best stable moiety by virtue of the extended 6π system; 6) Moreover, H_2BTA for controlling the molecular architectures, which in combination with appropriate outer- and inner-sphere ligands, allows the variation of physicochemical and explosive properties within a wide range.

As the integration of triazole and tetrazole, 3-(tetrazol-5-yl)triazole (H_2tztr), with high nitrogen content (N% = 71.54%), is quite a desirable ligand for assembling various HE-MOFs because of its unique advantages: 1) H_2tztr with a decomposition temperature of up to 300 ^{o}C possesses a rigid structural framework, which could improve the insensitivity and thermostability of the anticipated coordination compounds; 2) The H_2tztr ligand indicates abundant coordination modes, such as multidentate or bridging building blocks, offering the possibility for constructing unpredictable and fascinating MOFs.

1,2-bis(tetrazol-5-yl)ethane (H_2BTE) as a versatile ligand not only features excellent chemical stability, but also possesses richer coordination modes owing to the flexible and torsional C-C bond. H_2BTE has the potential to generate nitrogen-rich, highly endothermic metal salts with good performance and high thermal stability.

4,4'-azo-1,2,4-triazole (atrz) have the following advantages: 1) As a nitrogen-rich heterocyclic

ACCEPTED MANUSCRIPT

backbone [62], atrz possesses high nitrogen content (N% = 68.29%), high heat of formation (878 kJ mol^{-1}) and excellent thermal stability with a decomposition temperature up to 313 ^{o}C, which could enhance the energetic performances of the target compounds; 2) As a ligand, atrz has more than six potentially coordinated N atoms in a molecule, resulting in more bridging modes to meet the geometric requirements of 3D framework [63]; 3) Its decomposition predominantly generate environmentally benign nitrogen gases. Recent modeling and testing have indicated that the existence of high concentrations of nitrogen species in the combustion products of propellants can decrease gun barrel erosion through accelerating the formation of iron nitride rather than iron carbide on the interior surface of the barrel.

2.2 Triazine, tetrazine and their derivatives

Scheme 3 Triazine, tetrazine and their derivatives.

The high-nitrogen compounds above (Scheme 3) form a unique class of energetic materials. The high heat of formation is directly attributable to the large number of inherently energetic N-N and C-N bonds. What's more, the high-nitrogen ligands containing polyazides possess even higher heats of formation because their energy content rapidly increases with the number of energetic azido groups in the molecule.

2.3 Azide

Azide, a simple nitrogen-rich ligand with the highest nitrogen content of 100%, is a prominent energetic moiety which can increase the heat of formation by about 355 kJ·mol^{-1} and can be easily used to alter oxygen balance and the combustion product of azide is environmentally friendly. Furthermore, as a member of the short bridging ligand group, azide can link transition metal ions via multiple coordination modes. Additionally, azido has been studied due to its explosive nature because of its ability to form pure and mixed-ligand compounds, its ambidentate nature and bridging capacity and so on.

2.4 Hydrazine and its derivatives

Scheme 4 H ydrazine and its derivatives.

Hydrazine could be selected as ligand for HE-MOFs owing to its bidentate nature, exclusively

ACCEPTED MANUSCRIPT

gaseous decomposition products. The reaction of hydrazine with atmospheric carbon dioxide obtained an excellent candidate, hydrazine carboxylic acid (Scheme 4c), possessing at least three different coordination modes. The hidden source of carbon dioxide could decrease the energy content and density as well as desensitize the compound. The stabilizing and bridging hydrazinecarboxylate chelate sufficiently satisfies the design requirements for practical, stabilized polymeric energetic compounds.

2.4 Furazan (furoxan) and its derivatives

Scheme 5 Furazan (furoxan) and its derivatives.

Among these compounds (Scheme 5), furazan (furoxan) group is a unique class of heterocyclic compounds with various interesting properties, used as biologically active compounds [64] and high-energy materials [65]. Previous studies have revealed that a series of energetic compounds with excellent performances can be synthesized based on the furazan (furoxan) ring [66]. These compounds achieve an significant role in improving the performance of explosives owing to their high density, high positive heat of formation and good oxygen balance. Consequently, furazan (furoxan) compounds have been a burgeoning topic of intense interest. Especially, furoxan compounds possess better oxygen balance than furazan compounds [67,68]. What's more, a combination of the furoxan ring with other energetic groups or backbones bearing acidic protons, such as triazole, tetrazole or their derivatives, could serve as an anion after deprotonation or energetic ligand.

2.5 Energetic moieties

Scheme 6 Energetic moities.

The existences of energetic moities (Scheme 6) not only further improve the energetic performance, but also ameliorate oxygen balance of the whole system to fully release the energy.

3. 1D energetic MOFs

Accepted Manuscript

ACCEPTED MANUSCRIPT

Figure 1. The zigzag chain of **1**.

In 2005, the pioneering scientist, Thomas M. Klapötke, reported a bta-based compound (H_2bta = bis(tetrazolyl)amine), Cu(bta)$(NH_3)_2 \cdot H_2O$ (**1**) (ρ =1.9882 g·cm^{-3}, N% = 61.66%), showing 1D zigzag chains linked through the bta^{2-} ligands (Figure 1) [69]. The activation energy for compound **1** is 46.90 ± 0.16 kcal·mol^{-1}, indicating good thermal stability. Thermochemical properties have been calculated using the ICT thermodynamic code. The enthalpy of formation, critical temperature of thermal explosion, entropy of activation ($\Delta S^{\neq}$), enthalpy of activation ($\Delta H^{\neq}$) and free energy of activation ($\Delta G^{\neq}$) were obtained as -1150.1 K·mol^{-1}, 538.06 K, -172.08 J·K^{-1}·mol^{-1}, 220.32 kJ·mol^{-1} , and 311.07 kJ·mol^{-1} for **1**, respectively. For initial safety testing, the impact and friction sensitivity were tested according to BAM methods with the "BAM Fall hammer" and "BAM friction tester", classifying as insensitive toward impact (>40J) and friction (>360N).

Figure 2. An infinite one-dimensional coordination array polymer built from centroasymmetric mononuclear [Ag(MHT)(H_2O)] units and MHT bridges in **2**.

The nitrogen content of 5-(1-methylhydrazinyl)tetrazole (MHT) is 73.65%, which is nearly the same as the typical energetic nitrogen-rich tetrazole compound, bis(tetrazolyl)amine (H_2bta·H_2O, N=73.67%). The other pioneering scientist in energetic field, Jean'ne M. Shreeve, reported a compound of metal combined with the nitrogen-rich molecule MHT, $\{[Ag(MHT)]\cdot H_2O\}_n$ (**2**), possessing the high nitrogen content of 34.52% [9]. **2** exhibits an infinite 1D MOF structure (Figure 2) built from mononuclear [Ag(MHT)(H_2O)] units and MHT bridges. There is one water molecule in the crystal without any coordinated water molecules. The two adjacent MHT ligands are in opposite orientations. The density of **2** is up to 2.47 g·cm^{-3}. An analogous method was used to obtain the standard enthalpy of formation for **2** (-263 kJ·mol^{-1}). **2** is insensitive toward impact (>40 J).

Figure 3. Synthesis and 1D structure of $\{[Cu_n(ATZ)_3](ClO_4)_2\}_n$.

In 2010, Cudzilo *et al*. reported a 1D MOF with formula of $\{[Cu(ATZ)](ClO_4)_2\}_n$ (**3**, ATZ = 4-amino-1,2,4-triazole) in which Cu(II) cations are linked together by triple triazole bridges, surrounding with perchlorate anions in the external zone (Figure 3) [70]. It can be characterized as

ACCEPTED MANUSCRIPT

a comparatively stable (decomposes above 250 ^{o}C), low-sensitive to friction (10N) and high energetic detonation properties (6.5 km·s^{-1} at 1.4 g·cm^{-3}). Upon exposure to flame, it detonates in pressed charges of 200 mg in mass and initiates detonation of PETN charges. So that the compound may be used as an environmentally friendly and safe replacement of lead azide (LA) and lead styphnate (LS).

Figure 4. 1D chain structure of **4** along the Zn···Zn axis, surrounding with PA molecules in the external zone.

In 2013, employing the same ligands, $\{Zn(ATZ)_3](PA)_2 \cdot 2.5H_2O\}_n$ (**4**) (ATZ = 4-amino-1,2,4-triazole, PA = picrate) with the nitrogen contents of 30.77%, was synthesized and characterized by Zhang *et al* [21]. Crystal structure analysis shows that ATZ acting as bidentate ligands with N1 and N2 atoms connect with Zn(II) cations to form a 1D chain structure along the Zn···Zn axis (Figure 4), surrounding with PA molecules in the external zone. Thermal analysis indicated that some main endothermic and exothermic processes occurred in 50-600 ^{o}C corresponding to TG-DTG curves. Kissinger method and Ozawa method were applied to study the Kinetics parameters of the title compound. The enthalpy of formation, critical temperature of thermal explosion, entropy of activation ($\Delta S^{\neq}$), enthalpy of activation ($\Delta H^{\neq}$), and free energy of activation ($\Delta G^{\neq}$) were calculated and obtained as -1150.1K·mol^{-1}, 264.91 ^{o}C, -172.08 J·K^{-1}·mol^{-1}, 220.32kJ·mol^{-1}, and 311.07kJ·mol^{-1} for **4**, respectively. The impact sensitivity of **4** shows that h_{50} (the 50% firing height) was 56.7cm (27.8 J). More importantly for **4**, the heat of combustion (–11.30 MJ·kg^{-1}) was higher than that of RDX (–9.60 MJ·kg^{-1}), HMX (ca. -9.44 to 9.88 MJ·kg^{-1}), $[Mn(AZT)_4(H_2O)_2](PA)_2 \cdot 4H_2O$ (-10.39 MJ·kg^{-1}, AZT = 3-azido-1,2,4-triazole) and $[Co(AZT)_2(H_2O)_4](PA)_2$ (-8.77 MJ·kg^{-1}) [71]. In the end, compared to $[Cd(ATZ)_2(H_2O)_4](PA)_2$ [impact sensitivity: h_{50} = 18.63 cm (91.3 J), friction sensitivity: 24%, flame sensitivity: h_{50} = 12.17 cm] [72], compound **4** shows lower sensitivities.

Figure 5. The five-member and six-member rings give linear chains along *a* axis, thus, a 1-D coordination polymer

is formed, surrounding with NO_3^- anions in the external zone in **6**.

ACCEPTED MANUSCRIPT

Figure 6. A drawing of the 1D loop chain in **7**, surrounding with ClO_4^- anions in the external zone.

3-Hydrazino-4-amino-1,2,4-triazole (HATr, N% = 73.65%) increases two nitrogen atoms on the side of amine of ATZ, which is of interest as an energetic ligand to transitional metal compounds by Ilyushin and co-authors in 1993 [73]. In 2003, Ugryumov *et al* [74]. used the same ligand to prepare cobalt(II), copper(II), nickel(II) and cadmium(II) perchlorate compounds, in which the copper compound shows the most effective light-sensitive properties as a laser-ignition explosive. Ilyushin *et al* [75]. further studied the influence of various additives on the threshold of laser initiation of the copper perchlorate compound with HATr as a ligand in 2012. Furthermore, Zhang *et al*. synthesized two energetic MOFs through reaction with HATr ligands and metal ions, $[Mn_2(HATr)_4(NO_3)_4{\cdot}2H_2O]_n$ (**5**, N% = 46.12) and $[Cd_2(HATr)_4(NO_3)_4{\cdot}H_2O]_n$ (**6**, N% = 41.40), and studied through non-isothermal kinetic analysis, energies of combustion and enthalpies of formation [18]. HATr shows chelating and bridging coordination mode in above compounds. As an example for **6**, the five-member and six-member rings formed by one Cd ion and two HATr ligands give 1D chain along *a* axis (Figure 5). The non-isothermal kinetic analysis results indicate that the Arrhenius equations can be expressed as $\ln k = 10.48–134.5\times10^3/RT$ for **5** and $\ln k = 18.16–222.7\times10^3/RT$ for **6**. The energies of combustion and enthalpies of formation of **5** and **6** are -7186.25, -6922.53, -1002.35, and -457.27 $kJ{\cdot}mol^{-1}$, respectively. Recently, a 1D Cd(II) MOF was obtained, $[Cd(HATr)_2(ClO_4)_2]_n$ (**7**, N% = 31.12%, ρ = 2.240 $g{\cdot}cm^{-3}$) [20]. The HATr ligands are coordinated to Cd(II) metal centers in a tridentate chelating-bridging fashion to form the $\{Cd_2N_4\}$ six-membered ring, generating second building units (SBUs). These SBUs are interlinked each other to form a 1D looped chain structure (Figure 6). The onset decomposition temperature of **7** is 305 ^oC, showing good thermals stability. The critical temperature of thermal explosion, entropy of activation ($\Delta S^{\neq}$), enthalpy of activation ($\Delta H^{\neq}$), and free energy of activation ($\Delta G^{\neq}$) were calculated and obtained as 318.01 ^oC, -120.78 $J{\cdot}K^{-1}{\cdot}mol^{-1}$, 198.60 $kJ{\cdot}mol^{-1}$, and 268.28 $kJ{\cdot}mol^{-1}$ for **7**, respectively. The impact sensitivity of **7** (12.7cm, 1J) is comparable to that of LA (2–4 J).

Figure 7. One-dimensional chain structure of **8** viewed along the *a* axis of the unit cell.

In order to obtain the compounds with more complicated structure and higher nitrogen content, the mixed ligands were used. One of the most effective second ligand is azide because it possesses

ACCEPTED MANUSCRIPT

highest nitrogen content of 100% and diverse coordination modes. Thus a more nitrogen-rich coordination compound $Zn_3(ATZ)_6(N_3)_6$ (**8**) (ATZ = 4-amino-1,2,4-triazole, N% = 61.7%, ρ= 1.824 g·cm^{-3}) was prepared and characterized [19]. Octahedral zinc(II) cations are bridged by μ-1,1 bridging azido groups and two bidentate ATZ ligands to generate a 1D chain structure (Figure 7). The compound is insensitive to impact, flame and friction stimuli.

Figure 8. The one-dimensional chain structure along *a* axis in $[Cd(en)(N_3)_2]_n$ and octahedral coordination structure of Cd(II).

$[Cd(en)(N_3)_2]_n$ (**9**), shows that the Cd(II) ion is six-coordinated in a distorted octahedral geometry with four azido ligands by μ-1,1 azido bridges, and two ethylenediamine molecules which serve as bidentate ligands through nitrogen atoms (Figure 8) [76]. Thermal analysis indicates that there are two main successive exothermic processes between 245.85 ^{o}C and 427.85 ^{o}C as shown in the DSC curve. The thermal decomposition behavior of the title compound shows good thermal stability. The sensitivity measurement results indicate that $[Cd(en)(N_3)_2]_n$ has higher friction sensitivity and lower flame sensitivity compared to nickel(II) hydrazine azide.

Figure 9. A one-dimensional chain runs along *a* axis of the unit cell with alternating six-membered Zn–N4–Zn rings in **10**.

Zhang *et al*. reported azido and hydrazine based-energetic 1D MOF [77]. The energetic compound $[Zn(N_2H_4)_2(N_3)_2]_n$ (**10**) (ρ = 2.083 g·cm^{-3}, N% = 65.60%) was synthesized through $Zn(OAc)_2{\cdot}2H_2O$, hydrazine hydrate, and sodium azide in aqueous solution. A 1D chain runs along *a* axis of the unit cell with alternating six-membered Zn–N4–Zn rings (Figure 9). The experiment found that the combustion heat of the title compound is 5.45 MJ·kg^{-1}.

Figure 10. Crystal structure of NHP, surrounding with ClO_4^- anions in the external zone.

Figure 11. Structure of NHN, surrounding with NO_3^- anions in the external zone.

Chart 1. Energy of detonation for DFT-optimized structures ($\Delta E_{DFT,\ det}$) *vs* estimated heat of detonation (ΔH_{det}) from literature for 11 highly explosive materials (Values are from ref 78a for explosives **1**−**9** and ref 78b for explosives **10** and **11**. MF, mercury fulminate; ONC, octanitrocubane; other abbreviations are

ACCEPTED MANUSCRIPT

common explosive names.); (b) Bar diagram representation of the literature ΔH_{det} values for the 11 highly explosive materials along with the predicted ΔH_{det} for NHN, CHP, and NHP using the linear correlation developed in Chart 1a (a Also indicated are the error margins for the predicted values at the 95% confidence level. Both mass-density (kcal·g^{-1}) and volume-density (kcal·cm^{-3}) of the ΔH_{det} are indicated, and the heats are arranged in increasing order of volume-density.)

By virtue of a similar self-assembly strategy, three energetically unstable MOF materials, namely nickel hydrazine perchlorate (NHP, **11**), cobalt hydrazine perchlorate (CHP, **12**) and nickel hydrazine nitrate (NHN, **13**), were obtained. NHP and CHP adopt a linear polymeric motif utilizing only one bridging hydrazine (Figure 10), whereas NHN has a triply bridging hydrazine cage in the polymeric structure in which all hydrazine ligands bridge successive nickel centers (Figure 11) [10]. To estimate the heat of detonation (ΔH_{det}) of these three 1D MOFs (NHP , CHP and NHN), Hope-Weeks *et al*. adopted density functional theory (DFT) to compute the energy of detonation (ΔE_{det}), from which ΔH_{det} is estimated by using a linear correlation ($\Delta H_{det} = 1.127\Delta E_{det} + 0.046$, r = 0.968) developed from known ΔH_{det} data for eleven commonly used high explosives (Chart 1a). The DFT code DMol was employed [78c], with the electronic wave functions expanded in a double-numeric polarized basis set, while the exchange and correlation effects were incorporated through the gradient-corrected PBE functional [78d]. For a periodic calculation, an accurate Brillouin-zone sampling of the reciprocal lattice was also necessary. This was ensured by summation over a finite set of K-points chosen according to the Monkhorst−Pack scheme [78e] with a grid spacing of 0.05 Å^{-1}. The only published ΔH_{det} value for NHN, 1.014 kcal·g^{-1} (2.16 kcal·cm^{-3}) [78f], is within the error margin but close to the upper limit of their prediction. Both NHP and CHP exhibit good energetic properties with high heats of detonation comparable with that of the known explosives, such as CL-20, PETN, RDX, MF, lead azide and NHN, as shown in Chart 1b. Unfortunately, these nickel- and cobalt-based 1D MOFs are highly sensitive to flame, spark, and impact, which also precludes their commercial use.

4. 2D energetic MOFs

To explore the potential of advanced MOFs for further energetic applications, we investigated and discussed the 2D HE-MOFs.

ACCEPTED MANUSCRIPT

Figure 12. Six-coordinated Cu^{II} ions linked through the azido groups with μ-1,1,3 coordination mode to obtain 1D line in **14**.

The crystal structure of high-nitrogen energetic compound of copper(II) 1,2-diaminopropane (pn) azide, $[Cu(pn)(N_3)_2]_n$ (N% = 50.54%, ρ = 1.762 g·cm^{-3}) (**14**) shows that the azido groups display μ-1 and μ-1,1,3 coordination modes connecting with distorted octahedral Cu(II) ions to generate a 2D network (Figure 12) [23]. The heat of combustion of **14** is –4.43 MJ·kg^{-1}. The critical temperature of thermal explosion (T_b), entropy of activation ($S^{\neq}$), enthalpy of activation ($\Delta H^{\neq}$), and free energy of activation ($\Delta G^{\neq}$) of the decomposition reaction of **14** are 200.34 ^{o}C, -121.52 J·K^{-1} mol^{-1}, 165.06 kJ·mol^{-1}, and 221.26 kJ·mol^{-1}, respectively. The impact, friction, and flame sensitivities measuring results showed that **14** is insensitive to external stimuli.

Figure 13. The moleculars tructures of **15**. the slightly distorted-octahedral Cu1 cations are bridged azido groups with μ-1,1 bridging ligand and μ-1,1,3 coordination modes to obtain a 2D network.

In order to improve the density and nitrogen content of the above compound, one new multi-ligand 2D MOF of copper(II) ethylenediamine (en) azide, $[Cu_2(en)_2(N_3)_4]_n$ (N% = 53.98%, ρ =1.928 g·cm^{-3}) (**15**), was synthesized [22]. The slightly distorted-octahedral Cu(II) cations are bridged by azido groups with μ-1,1 bridging ligand and μ-1,1,3 coordination modes to obtain a 2D network (Figure 13). The experiment found that the energy of combustion, enthalpy of formation, the critical temperature of thermal explosion (T_b), the entropy of activation ($\Delta S^{\neq}$), enthalpy of activation ($\Delta H^{\neq}$), free energy of activation ($\Delta G^{\neq}$) of the decomposition reaction of **15** were -6.84 MJ·kg^{-1}, -1330,34 kJ·mol^{-1}, 152.13 ^{o}C, -204.70 kJ·mol^{-1}, 76.90 J·K^{-1}·mol^{-1}, and 160.12 kJ·mol^{-1}, respectively. The impact and flame sensitivity results showed that the 50% firing heights were 8.0 cm (7.84 J) and 15.0 cm (15.19J) for **15**, respectively.

Figure 14. The two zigzag chains linked by azido ligands are vertical to each other, and a novel two-dimensional rectangular-grid-like layer parallel to ab-plane of unit cell is formed in **16**.

In $[Cd(DAT)_2(N_3)_2]_n$ (**16**, DAT = 1,5-diaminotetrazole, N% = 63.42 %, ρ = 2.144 g·cm^{-3}), each center Cd(II) atom is six-coordinated with two trans DAT ligands and four trans μ-1,3 azido

ACCEPTED MANUSCRIPT

bridged ligands [79]. The two zigzag chains were linked by azido ligands to form a novel two-dimensional rectangular-grid-like layer (Figure 14). The thermal analysis shows that under nitrogen atmosphere with a heating rate of 10 $^{o}C \cdot min^{-1}$, the thermal decomposition of **16** starts just after the melting and yielding mainly environmentally friendly gases. It may be further studied in the field of energetic materials.

Figure 15. The six-coordinated Cd(II) cations are inter linked by μ-Cl ligands and HATr ligands to generate a 2D framework in **17**.

Two-dimensional Cd(II) MOF, $[Cd_2(NO_3)_2Cl_2(HATr)_2]_n$ (**17**, N% = 30.29%, ρ = 2.470 $g \cdot cm^{-3}$), shows that four nitrogen atoms (N7, N8, N7A and N8A) from two triazole rings bridge with two Cd1 atoms into a six-membered ring, and then the six-membered ring further bridges two Cd2 atoms through two nitrogen atoms (N1 and N2) from a triazole ring and one chloride ion (Cl1) to form a SBUs [20]. These SBUs are inter linked by μ-Cl ligands (Cl2) to construct a 2D square architecture as shown in Figure 15. Thermal behavior of the compound was investigated by DSC, which is thermally stable up to 249.85 ^{o}C. The critical temperature of thermal explosion (T_{bp}), entropy of activation ($\Delta S^{\neq}$), enthalpy of activation ($\Delta H^{\neq}$), and free energy of activation ($\Delta G^{\neq}$) of the decomposition reaction of **17** are 304.62 ^{o}C, -42.42 $J \cdot K^{-1} \cdot mol^{-1}$, 292.18 $kJ \cdot mol^{-1}$, and 316.28 $kJ \cdot mol^{-1}$, respectively.

Figure 16. 2D network with MHT anions as bridging ligands in **18**.

Copper Di-5-(1-methylhydrazinyl) tetrazolate, $Cu(MHT)_2$ (**18**, ρ = 2.031 $g \cdot cm^{-3}$), crystallizes in the monoclinic space group $P2_1/c$ by analysis of systematic absences, with two molecular moieties in each unit cell (Figure 16) [9]. The MHT anion displays delocalization of the negative charge because of bond homogenization. In the molecules of **18**, each Cu(II) ion is six coordinated, with an octahedral geometry. The MHT anion ligand is bidentate at the N1 and N7 positions while monodentate at the N4 position. **18** exhibits high nitrogen content of 58.01%. The enthalpy of formation of **18** (+93 $kJ \cdot mol^{-1}$) is higher than that of 0D Ag(I)-compound [56], because of the two nitrogen-rich MHT ligands coordinated to the center copper ion.

ACCEPTED MANUSCRIPT

Figure 17. Partial packing diagram of CHHP showing the sheet structure parallel to *bc* plane.

Figure 18. Partial packing diagram of a ZnHHP sheet showing the ladder motif. In both graphics, perchlorate anions and cocrystallized water have been omitted for clarity.

Chart 2. Bar chart representation of the literature ΔH_{det} values for eleven common explosive materials [64a,64b]. Previously reported values for CHP, NHP, and NHN, along with the predicted ΔH_{det} values for CHHP and ZnHHP are also shown. Error bars correspond to the 95% statistical-confidence level for these values.

The previously prepared NHP and CHP have highly sensitivity and extremely powerful-dangerous combination. Consequently, the need for another ligand would somewhat attenuate their energetic properties. The hydrazinecarboxylate as a bi- or tridentate ligand is apt to constructing the energetic MOFs. Two novel energetic cobalt- and zinc-based MOFs, $[Co_2(N_2H_4)_4(N_2H_3CO_2)_2]\cdot 2ClO_4\cdot H_2O$ (**19**, CHHP) and $[Zn_2(N_2H_4)_3(N_2H_3CO_2)_2]\cdot 2ClO_4\cdot H_2O$ (**20**, HHP), were reported [11]. CHHP is composed of distorted octahedral metal centers with mixed coordination spheres, in which each cobalt ion bears three hydrazine ligands and two hydrazine carboxylate ligands, whereas at the same time every hydrazine carboxylate ligand is a tridentate ligand that bridges two cobalt ions in the polymeric sheet structure (Figure 17). Similarly, energetic ZnHHP also form a 2D polymeric sheet structure (Figure 18), in which the zinc ion is octahedrally coordinated with four equatorial hydrazine ligands and two axial bonds to the oxygen atoms of the hydrazine carboxylate moiety. Both structures are composed of alternating layers of structurally stabilized metal organic fuel and oxidizing perchlorate anions. Their calculated crystal ion densities are ≥ 2.0 g·cm^{-3} at 150 K. CHHP and ZnHHP exhibit good thermal stabilities (decomposition temperatures of 231 ^{o}C and 293 ^{o}C, respectively), which are much higher than that of CHP (194 ^{o}C). As a result of these structural modifications, CHHP and ZnHHP possess much milder sensitivity profiles, compared to the highly sensitive 1D MOFs NHP and NHN, while retain higher energy content than typical metal-based explosives. To estimate the heat of detonation (ΔH_{det}) of these two new explosives and see how they compare with the ΔH_{det} values for common energetic materials, Hoop Weeks *et al*. adopted the methodology for NHP and CHP [10]. However, the variation in ΔH_{det} due to variation in the positions of ClO_4^- and water was

ACCEPTED MANUSCRIPT

found to be modestly more energetic than nickel hydrazine nitrate (NHN), the ionic polymer of reference from the previous study, while possessing considerably lower energetic output than reported for CHP and NHP (Chart 2). Such a decrease in heats of detonation is expected due to the lower perchlorate load and significantly increased structural stabilization coming from the chelating hydrazinecarboxylate anion and a network of hydrogen bonds between the parallel sheets of compounds. Nevertheless, CHHP and ZnHHP still outperform traditional metal-based energetics by delivering energetic output on the order of magnitude of common organic secondary explosives such as TNT, tetryl and FOX-7, while displaying moderate sensitivities, appropriate for convenient handling and intentional initiation. Therefore, these energetic 2D MOFs are excellent candidates for replacing heavy-metal primers such as lead azide.

Figure 19. Binuclear polymers with Pb···Pb 4.503 Å are bridged water O1 to generate 2D sheet viewed along *a* axis in **21**.

In our work, a Pb(II) compound with N,N-bis[1(2)H-tetrazol-5-yl]amine(H_2bta) ligand, $[Pb(bta)(H_2O)_2]_n$ (N% = 31.97%) (**21**), was reported by Chen *et al*., in which $[Pb(H_2O)_2]^{2+}$ units are joined by bta^{2-} spacers to generate a 1D zigzag chain with a period of 7.263 Å [25]. The density of **21** is up to 3.214 $g \cdot cm^{-3}$. If a limit of 2.90 Å is placed upon PbII–Ow, **1** is a binuclear polymer with Pb···Pb 4.503 Å. It thus results in a 2D layer (Figure 19) by bridging water O1. Compound **21** was explored as additives to promote the thermal decomposition of ammonium perchlorate (AP) by differential scanning calorimetry.

Figure 20. The 2D layer is formed based on the coordination of O with Pb(II) ion at the axial position in **22**.

Figure 21. The 2D layer, in which the adjacent Pb(II) centers are linked by the bridging H_2tztr ligand in two different directions to form a slightly distorted 2D (4, 4) sheet in **23**.

Two energetic compounds, $[Pb(Htztr)_2(H_2O)]_n$ (**22**) and $[Pb(H_2tztr)(O)]_n$ (**23**), were synthesized and then structurally characterized (N% = 39.4% for **22**, N% = 27.2% for **23**), showing the high density of 2.519 and 3.511 $g \cdot cm^{-1}$, respectively [16]. Thermogravimetric measurements demonstrated that the compounds possess excellent thermostabilities with high decomposition temperatures up to 340 ^oC for **22** and 318 ^oC for **23**, which are far greater than AP (T_{dec} = 245 ^oC)

ACCEPTED MANUSCRIPT

and RDX (T_{dec} = 204 °C). Structural analysis revealed that both compounds have reticular 2D structures. Remarkably, Figure 20 shows the 2D layer of **22**, in which the adjacent Pb(II) centers are linked by the bridging H_2tztr ligand in two different directions to form a nearly square grid. The non-bonding Pb···Pb distances are 9.247, 10.276, 9.814 and 9.814 Å, respectively. The internal angles of each grid are 82.798°, 90.599° and 88.716°, respectively, showing a slightly distorted 2D (4, 4) sheet. The H_2tztr ligands in **23** adopt the bidentate chelating and bridging modes and connect to two Pb(II) ions; the adjacent Pb(II) ions are linked by two bridging O atoms (O(1) and O(1b)) simultaneously to form a 1D chain. The 2D layer is formed based on the coordination of O(1a) with Pb(II) ion at the axial position (Figure 21). The heat of detonation of **22** (1.359 kcal·g^{-1}) locates at a higher level than the conventional explosives (HMX, RDX and TNT) and energetic MOFs (ATRZ-1 [12], ATRZ-2 [12], CHP, NHP, CHHP and ZnHHP), but the mediocre values of D (7.715 km·s^{-1}) and P (31.57 GPa) are probably due to the existence of the coordinated water molecule. The lower heat of detonation of compound **23** (0.255 km·s^{-1}) is attributed to the poor nitrogen content, in spite of the higher density which benets D (8.122 km·s^{-1}) and P (40.12 GPa). Therefore, replacing the water molecule in **22** or the oxygen atoms in **23** with energetic small organic molecules would improve the detonation performance without impacting on the structural stabilities of the compounds. Contrasting with the metallic oxides, the catalytic performance of the title compounds on the thermal decomposition of AP and RDX is mediocre and this is probably because the thermal decomposition temperatures of title energetic MOF are far greater than AP (T_{dec} = 245 °C) and RDX (T_{dec} = 204 °C), thus postponing the energetic release of two compounds.

Figure 22. The 2D layer-like structure is constructed by the interlinkages between Cu(I) ions and H_2tztr ligands in **24**.

Chart 3. Bar chart representation of the previously reported ΔH_{det} values for the common explosive materials, including CL-20 and ONC. Previously reported values for energetic MOFs (ZnHHP, CHHP, CHP, NHP, ATRZ-1, and ATRZ-2), along with the predicted ΔH_{det} value for **24** and **37** are also shown.

Furthermore, for our recent work, hydrothermal reaction of Cu(II)/Cu(I) with a rigid nitrogen-rich ligand, 3-(1H-tetrazol-5-yl)-1H-triazole (H_2tztr), led to a HE-MOFs: $[Cu(Htztr)]_n$ (ρ

ACCEPTED MANUSCRIPT

= 2.435 g·cm^{-3}, N % = 49.08%) (**24**) [17]. As shown in Figure 3b, the N1, N2, N3, and N5 atoms in the H_2tztr ligand adopt monodentate bridging modes to connect to four corresponding Cu(I) ions. In this way, the 2D layer-like structure is constructed by the interlinkages between Cu(I) ions and H_2tztr ligands, as shown in Figure 22. The compound **24** provides the unprecedented thermostability (355 ^{o}C), detonation velocity (10.40 km·s^{-1}) and detonation pressure (56.48 GPa) and heat of detonation (3.9582 kcal·g^{-1}). To the best of our knowledge, the ΔH_{det} value of **24** is unprecedentedly superior to the reported energetic MOFs and considerably higher than those of hexanitrohexaa-zaisowutzitane (CL-20; about 1.5 kcal·g^{-1}) [80a] and octanitrocubane (ONC; about 1.8 kcal·g^{-1}) [80b], known the most intense organic explosives (Chart 3). The brilliant ΔH_{det} of **24** is probably attributed to the high nitrogen content and rigid structural framework. For safety testing, the impact, friction and electrostatic sensitivities of the three compounds were investigated. The impact sensitivity of **24** is 32 J, whereas the impact sensitivity for TNT is 15 J under the same test conditions. Evidently, the impact sensitivity of **24** is lower than that of TNT and of the known energetic MOFs, such as ATRZ-1 (IS = 22.5 J). No friction sensitivities are observed up to 36 kg (360 N) for the compounds. In addition, the three compounds are more likely to be less sensitive to electrostatic discharge than both HMX and TNT. The finding exemplifies the potential application and advances in the integrated performance of MOF-based HEDMs.

Figure 23. In isostructural **25** and **26**, the chiral chain connects two adjacent opposite chiral ones by μ_2-κN3:κN4 tetrazolate groups to form an achiral 2D framework parallel to *bc* plane.

Hydrothermal reaction of N-(2-cyanoethyl)glycine and NaN_3 with corresponding metal salts yielded two energetic MOFs: $[M(tzeg)(H_2O)]_n$ (M = Cd^{2+} for **25**, Cu^{2+} for **26**) (H_2tzeg = N-[2-(1H-tetrazol-5-yl)ethyl]glycine) [24]. Nitrogen-rich $tzeg^{2-}$ ligand is a new in situ generated organic compound through [2+3] cycloaddition reaction of nitrile and azide, which adopts a μ_3-κO1:κO2,N5,N4:κN3 coordination fashion in **25** and **26**. In isostructural **25** and **26**, the chiral chain connects two adjacent opposite chiral ones by μ_2-κN3:κN4 tetrazolate groups to form an achiral 2D framework parallel to *bc* plane (Figure 23). For **25** and **26**, endothermic peaks are observed at 223 and 250 ^{o}C, respectively, corresponding to the loss of coordinated water molecules. The decomposition temperatures of **25** and **26** are 375 and 350 ^{o}C, respectively, on

ACCEPTED MANUSCRIPT

their onset DSC peaks, which can be proved sufficiently thermally stable compared to energetic materials. As nitrogen-rich energetic MOFs, **25** possesses higher enthalpy of combustion (ΔH_c), which are -11.583 $kJ \cdot g^{-1}$, than the classic energetic compounds 1,3,5-trinitro-1,3,5-triazacyclohexane (RDX, -9.6 $kJ \cdot g^{-1}$) and 1,3,5,7-tetranitro-1,3,5,7-tetraazacyclooctane (HMX, -9.44 to -9.88 $kJ \cdot g^{-1}$).

Figure 24. Polyhedral view of the 1D chain along *a* axis and 2D plane along *c* axis in **27**. [SrO6]: green triple prism;[SrO6N3]: red three-capped triangle prism. All H atoms are omitted for clarity.

Empolying the alkaline earth metal cations as the source of salts, in our work, two new energetic compounds, $[M(BTE)(H_2O)_5]_n$ (M = Sr(**27**), Ba(**28**)) [H_2BTE = 1,2-bis(tetrazol-5-yl)ethane], have been hydrothermally synthesized and structurally characterized [26]. They are isomorphous structure. In **27**, two Sr(II) ions with a distance of Sr···Sr of 4.2889(7) Å are bridged by two coordinated water molecules, forming a binuclear cluster $Sr_2H_{20}O_{10}$, which can be regarded as a SBU. These SBUs are connected by BTE ligands in mode II into a 1D zigzag chain long *a* axis, and the BTE ligands are further employed in mode I to link the near zigzag chains into a 2D plane along *c* axis (Figure 24). The flame color experiments and the effects of them on the thermal decomposition of AP are also explored, which reveal the two polymers not only display expected satisfactory colors but also show good catalytic activity toward decomposition of AP, indicating the potential applications of them for energetic materials as the ingredients or additives in pyrotechnics and propellants.

5. 3D energetic MOFs

Compared with 1D and 2D MOFs, 3D energetic structures possess more complicated connection modes and enhanced structural reinforcement.

Figure 25. The dimeric units of Cd_2N_2, $Cd_2(NNN)_2$, $Cd_2(NN)_2$ bridged through double μ-1, 1 azide bridges, μ-1, 3 azide bridges and bidentate bridging hydrazine ligands, respectively, to generate a 3D network structure in **29**.

Coordination polymer of cadmium(II) hydrazine azide, $[Cd_2(N_2H_4)_2(N_3)_4]_n$ (**29**, ρ =2.638 g

ACCEPTED MANUSCRIPT

cm^{-3}, N% = 49.04%), contains two crystallographically independent sets of distorted octahedral Cd(II) atoms and dimeric units of Cd_2N_2, $Cd_2(NNN)_2$, $Cd_2(NN)_2$ through double μ-1,1 azide bridges, μ-1,3 azide bridges and bidentate bridging hydrazine ligands, respectively, resulting in a 3D network structure (Figure 25) [81]. The sensitivity experimental results indicate that $[Cd_2(N_2H_4)_2(N_3)_4]_n$ is very insensitive to external stimuli compared to nickel(II) hydrazine azide.

Figure 26. Interweaving of left/righthanded helical chains leads to an achiral 3D framework with void helical channels which have an opening with a maximum diameter of 5.90 Å (atom-to-atom distance) with a screw axis along *c* axis in **30**.

In $[Zn(tzeg)]_n$ (**30**, N% = 29.86%), the $tzeg^{2-}$ ligands display the same μ_3-*κO1:κO2,N5,N4:κN1* coordination style like **25** and **26** to connect three Zn(II) atoms to form the infinite left/right-handed helical chains (Figure 26) [24]. The carboxylate group in $tzeg^{2-}$ ligand adopts a syn-anti coordination fashion bridging two Zn(II) atoms. Each type of helices is homochiral with a helical pitch of ca. 6.97 Å (atom-to-atom distance) along *c* axis. Each left-handed helical chain (or the right one) links four adjacent right-handed helical chains (or the left ones) by carboxylate O1 atom bound to Zn(II). Interweaving of left/righthanded helical chains leads to an achiral 3D framework with void helical channels which have an opening with a maximum diameter of 5.90 Å (atom-to-atom distance) with a screw axis along *c* axis (Figure 26). The decomposition temperature of **30** is 425 ^{o}C, on their onset DSC peaks, which can be proved sufficiently thermally stable compared to energetic materials. The constant-volume combustion heat (ΔU_c) of **30** was measured by oxygen bomb calorimetry, and the value was 12.054 $kJ \cdot g^{-1}$. The enthalpy of combustion (ΔH_c) of **30** calculated from the combustion equation is -12.041 $kJ \cdot g^{-1}$, which are higher than the reported enthalpies of combustion of RDX (-9.60 $kJ \cdot g^{-1}$) and HMX (-9.44 to -9.88 $kJ \cdot g^{-1}$), attributing to the nitrogen rich ligand and coordination effects resulting in close packing. The standard molar enthalpy of formation of **30** is calculated at 298.15 K using the Hess thermochemical cycle and combustion reactions, and deduced as -491.78 $kJ \cdot mol^{-1}$. Polymer **30** should have thermodynamically stable structures with lower enthalpy of formation, which can be safely stored, compared with highly sensitive explosives.

Figure 27. The 3D porous MOF of **31** depicted along the crystallographic *a* axis and the pores along *a* axis are

ACCEPTED MANUSCRIPT

filled with nitrate anions.

Figure 28. The 3D porous MOF of **32** depicted along the crystallographic *a* axis, and the pores along *a* axis are filled with nitrate anions.

Chart 4. Bar chart respresentation of the literature ΔH_{det} values for the common explosive materials including hexanitrohexaazaisowutzitane (CL-20), and octanitrocubane (ONC). Previously reported values for energetic MOFs (NHN, CHHP, ZnHHP, CHP, and NHP), along with the predicted ΔH_{det} values for **31** (ATRZ-1) and **32** (ATRZ-2) are also shown. Error bars correspond to the 95% statistical-confidence level for these values.

The latest contribution that addresses the preparation of 3D energetic MOFs described two energetic MOFs, $[Cu(atrz)_3(NO_3)_2]_n$ (**31**) and $[Ag(atrz)_{1.5}(NO_3)]_n$ (**32**) (atrz = 4,4'-azo-1,2,4-triazole), which were synthesized by a hydrothermal reaction in which atrz was used as an energetic multidentate ligand to link the metal ions (copper or silver ion) [12]. Compared to hydrazine, atrz has six potentially coordinating nitrogen atoms in the molecule, thereby meeting the geometric needs for a 3D architecture. Both 3D MOFs are air-stable and insoluble in most organic solvents, such as dimethyl sulfoxide, methanol, and acetone. Crystallographic studies revealed that $[Cu(atrz)_3(NO_3)_2]_n$ possessed a 3D porous MOF structure (Figure 27). Each atrz moiety served as a bidentate ligand bridging two Cu^{II} centers, thereby forming a 3D equilateral triangular porous framework (Figure 27). Interestingly, the pores along the *a* axis are filled with nitrate anions. The species, $[Ag(atrz)_{1.5}(NO_3)]_n$, also has a 3D irregular porous MOF structure, in which two types of pores are formed because the atrz ligand exhibited bonding to silver atoms in two different coordination modes. In this 3D structure (Figure 28), two types of pores (A and B) are formed parallel to the crystallographic *a* axis, and the bigger pores (A) host the NO_3^- anion. Two 3D energetic MOFs, $[Cu(atrz)_3(NO_3)_2]_n$ and $[Ag(atrz)_{1.5}(NO_3)]_n$, exhibited high densities (1.68 and 2.16 $g \cdot cm^{-3}$, respectively) and good thermal stabilities (decomposition temperatures of 243 and 257 ^oC, respectively). The strong structural reinforcement and extensive coordination networks in 3D frameworks may be responsible for their high thermal stabilities. More importantly, these energetic 3D MOF materials exhibit much lower sensitivity towards impact, friction, and electrostatic discharge than 1D and 2D energetic MOFs. To estimate

ACCEPTED MANUSCRIPT

the heat of detonation of these two new explosives and see how they compared with the heat of detonation (ΔH_{det}) values for 1D MOFs, 2D MOFs, and common energetic materials, Pang *et al*. adopted the same methodology recently for NHP and CHP [10,11]. The heat of detonation of compound **31** is 3.62 kcal·g^{-1} (6.08 kcal·cm^{-3}), which is even higher than those of CL-20 (about 1.5 kcal·g^{-1}) [80a] and octanitrocubane (ONC; about 1.8 kcal·g^{-1}) [80b], as shown in Chart 4. The relatively high heat of detonation could result from the nitrogen-rich heterocyclic ligand and the fascinating structure motifs, like CL-20 and its derivatives [82], these 3D cage compounds have high strain energies locked in the molecules, and it is released as an additional energy on detonation. Compound **31** exhibits the high heat of detonation, while retaining good stability, which makes it a competitive highly energetic material. The concept of 3D energetic MOFs thus provides a new insight for future developments of new-generation high-performance primary explosives.

Figure 29. 3D mixed valence CoIII–CoII energetic MOF with channels incorporating the latticed water molecules in **33**.

Chart 5. Bar chart representation of the literature ΔH_{det} values for the common explosive materials, including CL-20 and ONC. Previously reported values for energetic MOFs (ZnHHP, CHHP, CHP, NHP, ATRZ-1, and ATRZ-2), along with the predicted ΔH_{det} value for 2 are also shown. Error bars correspond to the 95% statistical-confidence level for these values.

Reaction of Co(II) with the nitrogen-rich ligand N,N-bis(1H-tetrazole-5-yl)-amine (H_2bta) leads to an insensitive MOF-based energetic compound (N%=51.78 %, IS>40 J), $[Co_9(bta)_{10}(Hbta)_2(H_2O)_{10}]_n \cdot [22(H_2O)]_n$ (**33**), which exhibits a 3D mixed valence Co^{III}-Co^{II} energetic MOF with channels incorporating the latticed water molecules [13]. Four different kinds of coordination fashions of bta^{2-} exist in the title compound, namely, μ_2-1,1′:4′, μ_3-1,1′:3:3′, μ_3-1,1′:3:4′ and μ_3-1,1′:4:4′. These ligands employ such chelating-bridging coordination modes, linking Co^{III} and Co^{II} centers to form the 3D porous MOF with channels incorporating guest water molecules connected with the nitrogen atoms from tetrazole rings by hydrogen-bonding interactions (Figure 29). Furthermore, a new energetic compound (N%=59.85 %, IS=27 J), $[Co_9(bta)_{10}(Hbta)_2(H_2O)_{10}]_n$ (**34**), was readily prepared by dehydration of **33**. Compound **33** was

ACCEPTED MANUSCRIPT

thermohydrated to produce a new, stable, energetic material with the nitrogen content of 59.85% and heat of denotation of 4.537 kcal·cm^{-3}, $[Co_9(bta)_{10}(Hbta)_2(H_2O)_{10}]_n$ (**34**). Sensitivity tests show that **34** is more sensitive to external stimuli than **33**, reflecting guest-dependent energy and sensitivity of 3D, MOF-based, energetic materials. Less-sensitive **33** can be regarded as a more safe form for storage and transformation to sensitive **34**. The detonation pressure (P) and detonation velocity (D) of **34** were calculated to be 32.18 GPa and 8.657 km·s^{-1} by Kamlet-Jacbos (K-J) equations; these numbers are slightly inferior to those of NHP and ATRZ-1, among the known energetic MOFs. The noticeably high values for ΔH_{det} of compound **34** are superior to the reported energetic MOFs (e.g., ZnHHP, CHHP, CHP, NHP, and ATRZ-2), except for ATRZ-1 in which a large number of nitrate ions fill the channels. For **34**, ΔH_{det} =2.658 kcal·g^{-1} (4.537 kcal·cm^{-3}); even higher than those of hexanitrohexaazaisowutzitane (CL-20; about 1.5 kcal·g^{-1}) [80a] and octanitrocubane (ONC; about 1.8 kcal·g^{-1}) [80b], which are the most intense organic explosives known (Chart 5). The relatively high ΔH_{det} value is attributed to the nitrogen-rich heterocyclic ligand and the attractive structure framework. As proposed, there is high-strain energy fixed in the 3D MOF-based energetic materials, which is released as an extra energy on detonation. The results of the sensitivity experiments indicate that **34** presents more violent sensitivity compared with **33**. Fortunately, **34** with high nitrogen content (N%=59.85%) maintains good thermal stability up to 253 °C and superior detonation performance. The results reveal that the two compounds are insensitive to external stimuli due to the stabilized, 3D, covalent framework, in which the molecules are more rigid than in the 1D or 2D structures. Obviously, the sensitivity difference between **33** and **34** is related to the guest-water-molecules effect. In this case, a large amount of the lattice water molecules in **33** decrease the sensitivity compared with **34**. More importantly, it presents an ingenious design to gain guest-dependent, 3D, MOF-based, energetic materials and examples a practical strategy for the storage and transportation of high-energy materials.

Figure 30. 3D network in **35** extended based on the 1D $Na_2(azole)_2$-SBU beetle-like chains.

Chart 6. Bar chart representation of the literature ΔH_{det} values for the common explosive materials including Previously reported values for energetic MOFs (HMX, RDX, TNT, ATRZ-1, ATRZ-2, CHP, NHP,

ACCEPTED MANUSCRIPT

CHHP, and ZnHHP), along with the predictedΔH_{det} value for **35** is also shown. Error bars correspond to the 95% statistical-confidence level for these values.

A reticular 3D heterometallic MOFs, $[Cu_4Na(Mtta)_5(CH_3CN)]_n$ (**35**) (N% = 40.08%), has been synthesized with 5-methyl tetrazole (Mtta) as ligand formed by acetonitrile and azide through in-situ synthesis and structurally characterized by X-ray single crystal diffraction [14]. The fluorescence spectrum demonstrates that **35** undergoes interesting structural transformation in aqueous, yielding the compound $[Cu_4Na(Mtta)_5H_2O]_n$ (**36**) confirmed by ^{1}HNMR, IR and PXRD. Thermoanalysis shows that **35** possesses excellent thermostability up to 335 ^oC. All of the Mtta ligands show μ_4-mode to coordinate with four metal ions. We notice in the framework that two adjacent sodium atoms can always be co-bridged by a pair of tetrazolate ligands using neighboring N atoms to generate a secondary building unit of sodium-tetrazolate, acting as a binuclear $Na_2(azole)_2$-SBU. The $Na_2(azole)_2$-SBU "connector" is sufficiently rigid due to two sodium atoms are locked by two tetrazolates, forming coplanar five-six-five membered rings. The μ_4-η^1:η^1:η^1:η^1 coordination mode of Mtta is crucial for the construction of **35**. Three Mtta ligands and twelve Cu atoms are assembled to from a beetle-like structure. One type of Mtta ligand links four Cu(I) ions to generate a beetle-like ribbon chain, while another type bridges two Cu(I) ions and two Na(I) ions, generating the $Na_2(azole)_2$-SBU chain. Consequently, the $Na_2(azole)_2$-SBU chains and the beetle-like chains interconnect to form a 3D framework (Figure 30). It is because of the 3D polymerized structure that endows **35** of structural reinforcement with good thermostability, and possible insensitivity. The test shows that the impact sensitivity value of the compound is 185 cm, which corresponds to the impact energy of 36 J. Under the same test condition, the impact sensitivity value (h_{50}) of TNT is 76.5cm (15.0 J). Consequently, the impact sensitivity of title compound is lower than that of TNT. Friction sensitivity of the compound is measured by applying a Julius Peter's machine using 20 mg sample. No friction sensitivity is observed up to 36 kg (360 N). The friction sensitivity of the compound is lower than that of RDX 12 kg. According to Hess's law, the standard molar enthalpy of formation of **35** at 298.15 K is calculated to be (182.92 ± 2.16) kJ mol^{-1}. The heat of detonation of compound **35** is 2.3657 kcal·g^{-1} (4.6723 kcal·cm^{-3}) which is higher than those of CL-20 (about 1.5 kcal·g^{-1}) and ONC (about 1.8 kcal·g^{-1}) [72]. In particular, the excellent heat of detonation (ΔH_{det}) only lower than that of ATRZ-1, the 3D

ACCEPTED MANUSCRIPT

energetic MOF reported previously. The result above demonstrates that **35** could be classified as top energetic MOFs. The high heat of detonation could result from the nitrogen-rich heterocyclic ligand and the complicated structure motifs, the 3D compound has high strain energy locked in the molecule, and it is released as an additional energy on detonation. The detonation pressure of **35** is 24.43 GPa (corresponding TNT 19.53 GPa and PETN 31.39 GPa). Detonation velocity is 7.225 $km \cdot s^{-1}$ (corresponding TNT 6.881 $km \cdot s^{-1}$ and PETN 8.564 $km \cdot s^{-1}$). The calculated properties coupled with the rather high thermal stability suggest that this high-nitrogen material may be attractive candidate for energetic applications. Compound **35** possesses good thermostability (T_c = 335 ^oC) and insensitivity. The standard molar enthalpy of formation for the compound is calculated to be (182.92 ± 2.16) $kJ \cdot mol^{-1}$. Importantly, the compound shows the explosion performances with the heat of detonation of 2.3657 $kcal \cdot g^{-1}$. The remarkable preliminary results indicate that compound **35** behaves as potential HEDM with favorable safety.

Figure 31. 3D porous structure of **36** of which the pores are filled with lattice water molecules.

In compound **36**, $\{[Cu(tztr)] \cdot H_2O\}_n$, the N1 and N2 atoms in the H_2tztr ligand adopt chelating modes to connect to one Cu(II) ion, whereas the N3, N4, and N5 atoms adopt monodentate bridging modes to link with three corresponding Cu(II) ions [17]. The porous 3D structural framework is obtained by the combination of Cu(II) ions and H_2tztr ligands, of which the pores are filled with lattice water molecules (Figure 31). The phase purity of the bulk materials are confirmed by X-ray powder diffraction (XRPD). The densities are identified as 2.435 $g \cdot cm^{-3}$ for **36** on the basis of experimental method using Automatic Density Analyzer. Compared with known energetic MOFs, the nitrogen contents of the three title compounds was 49.08% for **36**, only slightly lower than ATRZ-1 (N%=53.35%). The decomposition temperature of main frameworks in **36** were measured to be 355 ^oC, respectively, which are higher than that of HMX (287 ^oC), one of the most energetic materials commonly employed [69,70], and those of known energetic MOFs. The brilliant ΔH_{det} of **36** (3.9582 $kcal \cdot g^{-1}$), is probably attributed to the high nitrogen content and rigid structural framework, whereas the relatively low values of **36** are derived from an effect of lattice water molecules. The D and P of compound **36** are calculated to be 10.40 $km \cdot s^{-1}$ and 56.48 GPa, respectively, which have an absolute advantage over those of the

ACCEPTED MANUSCRIPT

known energetic MOFs, including ATRZ-1. Compared with the energetic MOFs reported previously, the compound **36** is insensitive to the external stimulus. It is probable that the tight integration between the rigid ligands and metal ions generates stable and insensitive structural frameworks.

Figure 32. Adjacent Cu(II) ions are linked by an azide bridge in m-1,1 (or end-on, EO) mode and a carboxylate bridge in *syn–syn* mode, yielding a formal 1D chain along the crystallographic a direction. Furthermore, nitro groups on the intrachain 3,5-DNBA molecules are connected to Cu(II) ions from other chains, forming a three-dimensional network structure in **37**.

3D energetic coordination polymer of azide-Cu(II), Cu(3,5-DNBA)(N_3) (**37**), was synthesized and structurally characterized by single crystal X-ray diffraction, where 3,5-DNBA represents 3,5-dinitrobenzoic acid [15]. Structural analysis reveals that the central Cu(II) ion coordinates with two azide anions and three 3,5-dinitrobenzoic acid anions to form a five-coordinated tetragonal pyramid structure. Adjacent Cu(II) ions are linked by an azide bridge in μ-1,1 (or end-on, EO) mode and a carboxylate bridge in *syn–syn* mode, yielding a formal 1D chain along the crystallographic *a* direction. Finally, nitro groups on the intrachain 3,5-DNBA molecules are connected to Cu(II) ions from other chains, forming a 3D network structure (Figure 32). It is noteworthy that one oxygen atom in the nitro group coordinates to Cu(II), which is rare in compounds with nitro groups. The as-prepared compound showed abrupt thermal decomposition at 268 ^{o}C, representing explosive performance and superior thermostability based on DSC and TG-DTG analyses. The result of non-isothermal kinetics analysis shows that the apparent activation energy is 301.05 kJ·mol^{-1}. The enthalpy of combustion of the compound is higher than those of RDX and HMX. The compound shows superior thermostability and insensitivity compared to RDX and TNT. The results above show that the compound is an example of a green, and high energy and insensitivity material.

Conclusion and perspective

Through the self-assembly of high-energy bridging ligands with metal ions, meanwhile, with the developments of measurement methods, theory calculation and simulation, the success in the

ACCEPTED MANUSCRIPT

preparation and characterization of HE-MOFs has been phenomenal. In fact, the high-energy bridging ligands not only provide the source of energy, but also exhibit the abundant coordination modes and obtain the different dimensional frameworks from 1D to 3D, possessing the desired physicochemical properties. For HE-MOFs, the choice of metal ions and the structural modification of energetic ligands will significantly influence the structures of the resulting MOFs and ultimately the energetic properties of the material. Significantly, metal ions, such as Pb^{2+}, Cd^{2+} and other heavy metal ions, exist potentially serious harm to human and environment, thus more attention should been paid to the aftertreatment of explosion products. Additionally, compared with 1D linear and 2D layered structures, 3D frameworks contain more complicated connection modes, which can further enhance structural reinforcement. More interestingly, some 3D HE-MOFs with porous structure incorporate a variety of energetic moieties such as nitrate anions (NO_3^-) and perchlorate anions (ClO_4^-) into channels or cages, hence improving the stabilities and energetic properties. Sometimes, the free water molecules incorporating in channels of 3D MOFs have a great influence on controlling the sensitivity and energy through dehydration and hydration interaction. On the other hand, the energetic moieties with oxygen-containing groups also ameliorate oxygen balance of the whole system to fully release the energy. Indeed, this new concept of designing HE-MOFs will provide a great opportunity for developing new-generation green primary explosives with predictable energetic performance of the target materials, which had been affirmed by Jean'ne M. Shreeve in 2014 [6].

To estimate the heat of detonation (ΔH_{det}) of these HE-MOFs reported recently, most of researchers adopted density functional theory (DFT) to compute the energy of detonation (ΔE_{det}), from which ΔH_{det} is estimated by using a linear correlation developed from known ΔH_{det} data for eleven common high explosives. The detonation velocity and detonation pressure were evaluated by the empirical Kamlet formula or the thermochemical code CHEETAH. Experimentally, the standard molar enthalpies of formation were obtained from the determination of constant-volume combustion energies, which is also used to calculate the detonation velocity and detonation pressure through the empirical Kamlet formula. Sensitivity testes, such as impact sensitivity, friction sensitivity, electrostatic sensitivity and so on, were measured through respective methods. The relevant data of compounds in this review have been summarized in table 1. Actually, although many groups have made some achievements, the pursuit of high performance and low

ACCEPTED MANUSCRIPT

sensitivity is the eternal theme of energetic materials, guiding to synthesize HE-MOFs with more excellent properties through the experimental method and the theoretical calculation. All in all, the more accurate, comprehensive and systematic measurement methods, theory calculation and theory simulation are needed to develop for studying HE-MOFs.

Furazan (furoxan) ligands with high density, high positive heat of formation and good oxygen balance contain more priority to improve the performance of explosives. Especially, the furoxan rings conjugated with tetrazoles or triazole, possessing the excellent characteristics of the both functional groups, is propitious to constructing high-dimensional energetic frameworks with more outstanding physicochemical properties. Synthesizing the ligands above, undoubtedly, is also a feasible and promising route to construct the HE-MOFs.

As known, a lot of reported MOFs with magnetic, catalytic, luminescent properties or absorption properties perform high nitrogen content, high density, low sensitivity, superior thermal stability as well as controllable property and structure, of which the potential energetic applications are neglected in the literatures. In the near future, the multifunctional materials would be achieved along the way of thought.

Moreover, the successful realization of nanoscale MOFs with controllable size, morphology and adjustable property has provided a very bright promise for developing new energetic nanomaterials. It is thus expected that nanoscale HE-MOFs would be implemented to optimize the related physicochemical properties, such as sensitivity and energetic performance.

Acknowledgements

We gratefully acknowledge financial support from the National Natural Science Foundation of China (grant no. 21373162, 21463020, 21073142，21203149 and 21173168), the Natural Science Foundation of Shanxi Province (grant no. 11JS110, 2013JM2002 and SJ08B09) and the Postgraduate Innovation Foundation of Northwest University (YZZ13046).

References

[1] L.E. Kreno, K. Leong, O.K. Farha, M. Allendorf, R.P.V. Duyne, J.T. Hupp, Chem. Rev. 112 (2012) 1105-1125;

ACCEPTED MANUSCRIPT

[2] M.C. Das, S. Xiang, Z. Zhang, B. Chen, Angew. Chem. Int. Ed. 50 (2011) 10510-10520.

[3] S.S. Nagarkar, B. Joarder, A.K. Chaudhari, S. Mukherjee, S.K. Ghosh, Angew. Chem. Int. Ed. 52 (2013) 2881-2885.

[4] Y. Bae, R.Q. Snurr, Angew. Chem. Int. Ed. 50 (2011) 11586-11596.

[5] C. Wang, D. Liu, W. Lin, J. Am. Chem. Soc. 135 (2013) 13222-13234.

[6] (a) Q.H. Zhang, J.M. Shreeve, Angew. Chem. Int. Ed. 53 (2014) 2540-2542;

[7] (a) N. Yanai, W. Kaneko, K. Yoneda, M. Ohba, S. Kitagawa, J. Am. Chem. Soc. 129 (2007) 3496-3497; (b) C. Wang, T. Zhang, W. Lin, Chem. Rev. 112 (2012) 1084-1104.

[8] (a) B. Manna, A.K. Chaudhari, B. Joarder, A. Karmakar, S.K. Ghosh, Angew. Chem. Int. Ed. 52 (2013) 998-1002; (b) J.H. Wang, M. Li, D. Li, Chem. Sci. 4 (2013) 1793-1801; (c) N. Yanai, K. Kitayama, Y. Hijikata, H. Sato, R. Matsuda, Y. Kubota, M. Takata, M. Mizuno, T. Uemura, S. Kitagawa, Nature Mater. 10 (2011) 787-793;

(d) S.B. Choi, H. Furukawa, H.J. Nam, D.Y. Jung, Y.H. Jhon, A. Walton, D. Book, M. O'Keeffe, O.M. Yaghi, J. Kim, Angew. Chem. Int. Ed. 51 (2012) 8791-8795.

[9] G.H. Tao, D.A. Parrish, J.M. Shreeve, Inorg. Chem. 51 (2012) 5305-5312.

[10] O.S. Bushuyev, P. Brown, A. Maiti, R.H. Gee, G.R. Peterson, B.L. Weeks, L.J. Hope-Weeks, J. Am. Chem. Soc. 134 (2012) 1422-1425.

[11] O.S. Bushuyev, G.R. Peterson, P. Brown, A.Maiti, R.H. Gee, B.L. Weeks, L.J.Hope-Weeks, Chem. Eur. J. 19 (2013) 1706-1711.

[12] S. Li, Y. Wang, C. Qi, X. Zhao, J. Zhang, S. Zhang, S.P. Pang, Angew. Chem. Int. Ed. 52 (2013) 14031-14035.

[13] S. Zhang, X.Y. Liu, Q. Yang, Z.Y. Su, W.J. Gao, Q. Wei, G. Xie, S.P. Chen, S.L. Gao, Chem. Eur. J. 20 (2014) 7906-7910.

[14] Y.Y. Feng, X.Y. Liu, L.Q. Duan, Q. Yang, Q. Wei, G. Xie, S.P Chen, X.W Yang, S.L. Gao, Dalton Trans. 44 (2015) 2333-2339.

[15] X.Y. Liu, Q. Yang, Z.Y. Su, S.P. Chen, G. Xie, Q. Wei, S.L. Gao, RSC Adv. 4 (2014) 16087-16093.

[16] W.J. Gao, X.Y. Liu, Z.Y. Su, S. Zhang, Q. Yang, Q. Wei, S.P. Chen, G. Xie, S.L. Gao, J. Mater. Chem. A, 2 (2014) 11958-11965.

[17] X.Y. Liu, W.J. Gao, P.P. Sun, Z.Y. Su, S.P. Chen, Q.Wei, G. Xie, S.L. Gao, Green Chem. 17 (2015) 831-836.

[18] (d) C.X. Xua, X. Yin, X. Jin, P. He, J. Qin, J.G. Zhang, J.S. Jiao, J. Coord. Chem. 67 (2014) 2004-2015.

[19] W.C. Tong, L. Yang, B.D. Wu, T.L. Zhang, Z. Anorg. Allg. Chem. 640 (2014) 980-985.

[20] C.X. Xu, J.G. Zhang, X. Yin, X. Ji, T. Li, T.L. Zhang, Z.N. Zhou, J. Solid. State. Chem. 226 (2015) 59-65.

[21] (a) B.D. Wu, T.L. Zhang, Y.L. Li, W.C. Tong, Z.N. Zhou,J.G. Zhang, L. Yang, Z. Anorg. Allg. Chem. 639 (2013) 2209-2215;

[22] B.D. Wu, Z.N. Zhou, F.G. Li, L. Yang, T.L. Zhang, J.G. Zhang, New J. Chem. 37 (2013) 646-653.

[23] B.D. Wu, Y.G. Bi, F.G. Li, L. Yang, Z.N. Zhou, J.G. Zhang, T.L. Zhang, Z. Anorg. Allg. Chem. 640 (2014) 224-228.

[24] S.H. Wang, F.K. Zheng, M.F. Wu, Z.F. Liu, J. Chen, G.C. Guo, A.Q. Wu, CrystEngComm, 15 (2013) 2616-2623.

[25] W.T. Wang, S.P. Chen, S.L. Gao, Eur. J. Inorg. Chem. (2009) 3475-3480.

Accepted Manuscript

ACCEPTED MANUSCRIPT

[26] Z.Q. Xia, S.P Chen, Q. Wei, C.F. Qiao, J. Solid. State. Chem.184 (2011) 1777-1783.

[27] D.M. Badgujar, M.B. Talawar, S.N. Asthana, P.P. Mahulikar, J. Hazard. Mater. 151 (2008) 289-305.

[28] M.B. Talawar, R. Sivabalan, T. Mukundan, H. Muthurajan, A.K. Sikder, B.R. Gandhe, A.S. Rao, J. Hazard. Mater. 161 (2009) 589-607.

[29] R. Wang, H. Xu, Y. Guo, R. Sa, J.M. Shreeve, J. Am. Chem. Soc. 132 (2010) 11904-11905.

[30] D. Fischer, T.M. Klapötke, J. Stierstorfer, Angew. Chem. Int. Ed. 53 (2014) 8172-8175.

[31] H. Gao, J.M. Shreeve, Chem. Rev. 111 (2011) 7377-7436.

[32] T.M. Klapötke, F.A. Martin, J. Stierstorfer, Angew. Chem. Int. Ed. 50 (2011) 4227-4229.

[33] Y.H. Joo, J.M. Shreeve, Angew. Chem. Int. Ed. 49 (2010) 7320-7323.

[34] P. Yin, J. Zhang, C. He, D.A. Parrish, M.S. Jean'ne, J. Hazard. Mater. 2 (2014) 3200-3208.

[35] L. He, G.H. Tao, D.A. Parrish, M.S. Jean'ne, Chem. Commun. 49 (2013) 10329-10331.

[36] Y.C. Li, C. Qi, S.H. Li, H.J. Zhang, C.H. Sun, Y.Z. Yu, S.P. Pang, J. Am. Chem. Soc. 132 (2010) 12172-12173.

[37] R. Deblitz, C.G. Hrib, S. Blaurock, P.G. Jones, G. Plenikowski, F.T. Edelmann, Inorganic Chemistry Frontiers. 1 (2014) 621-640.

[38] Y.Guo, H. Gao, B. Twamley, J.M. Shreeve, Adv. Mater. 19 (2007) 2884-2888.

[39] (a) L. Liang, H. Huang, K. Wang, C. Bian, J. Song, L. Ling, Z. Zhou, J. Mater. Chem. 22 (2012) 21954-21964; (b) M.H.V. Huynh, M.A. Hiskey, J.G. Archuleta, E.L. Roemer, R. Gilardi, Angew. Chem. Int. Ed. 43 (2004) 5658-5661; (c) M.H.V. Huynh, M.A. Hiskey, E.L. Hartline, D.P. Montoya, R. Gilardi, Angew. Chem. Int. Ed. 43 (2004) 4924-4928; (d) M.H.V. Huynh, M.A. Hiskey, D.E. Chavez, D.L. Naud, R.D. Gilardi, J. Am. Chem. Soc. 127 (2005) 12537-12543; (e) J. Kerth, S. Löbbecke, Propellants, Explos. Pyrotech. 27 (2002) 111-118; (f) D.R. Miller, D.C. Swenson, E.G. Gillan, J. Am. Chem. Soc. 126 (2004) 5372-5373; (g) M.B. Talawar, R. Sivabalan, N. Senthilkumar, G. Prabhu, S.N. Asthana, J. Hazard. Mater. 113 (2004) 11-25; (h) C. Ye, H. Gao, J.A. Boatz, G.W. Drake, B. Twamley, J.M. Shreeve, Angew. Chem. Int. Ed. 45 (2006) 7262-7265; (i) L. Liang, K. Wang, C. Bian, L. Ling, Z. Zhou, Chem. Eur. J. 19 (2013) 14902-14910.

[40] H. Chen, T. Zhang, J. Zhang, X. Qiao, K. Yu, J. Hazard. Mater. 129 (2006) 31-36.

[41] J.G. Zhang, J.Y. Li, Y. Zang, Y.J. Shu, T.L. Zhang, L. Yang, P.P. Power, Z. Anorg. Allg. Chem. 636 (2010) 1645-1647.

[42] W.C. Tong, J.C. Liu, Q.Y. Wang, L. Yang, T.L. Zhang, Z. Anorg. Allg. Chem. 640 (2014).2991-2997.

[43] T.L. Zhang, B.D. Wu, L. Yang, Z.N. Zhou, J.G. Zhou, Chin. J. Energy. Mater. 21 (201) 137-151.

[44] F.Q. Bi, X.Z. Fan, C. Xu, B.Z. Wang, Y.F. Zheng, Z.X. Ge, Q. Liu, Chin. J. Energy. Mater. 20 (2012) 805-811.

[45] X.J. Zhang, Y.C. Li, W. Liu, Y.Z. Yang, L. Peng, S.P. Pang, Chin. J. Energy. Mater. 20 (2012) 491-500.

[46] R.H. Ju, X.Z. Fan, H.J. Wei, F.Q. Bi, J.Z. Li, H. Wang, X.L. Fu, B.Z. Zhou, Chem. Propel. & Polym. Mater. 11 (2013) 23-28.

[47] J.Q. Xu, B.K. Shang, W. Wang, F. Liu, L.X. Wang, Chem. Propel. & Polym. Mater. 9 (2011) 91-98.

Accepted Manuscript

ACCEPTED MANUSCRIPT

[48] T.Z. Zhang, X.J. Feng. T.B. Zhu, C.C. Miao, H.Q. Ma, Chem. Propel. & Polym. Mater. 11 (2013) 1-5.

[49] H.S. Huang, T.L. Zhang, J.G. Zhang, L.Q. Wang, J. Hazard. Mater. 179 (2010) 21-27.

[50] M.B. Talawar, R. Sivabalan, T. Mukundan, H. Muthurajan, A.K. Sikder, B.R. Gandhe, A. Subhananda Rao, J. Hazard. Mater. 161 (2009) 589-607.

[51] D.E. Chavez, M.A. Hiskey, J. Energ. Mater. 17 (1999) 357-377.

[52] M.B. Talawar, R. Sivabalan, T. Mukundan, H. Muthurajan, A.K. Sikder, B.R. Gandhe, A.S. Rao, J. Hazard. Mater. 161 (2009) 589-607.

[53] T.M. Klapötke, Chemistry of High Energy Materials, Walter de Gruyter, Berlin/New York, 2011.

[54] P.F. Pagoria, G.S. Lee, A.R. Mitchell, R.D. Schmidt, Thermochim. Acta. 384 (2002) 187-204.

[55] R.P. Singh, R.D. Verma, D.T. Meshri, J.M. Shreeve, Angew. Chem. Int. Ed. 45 (2006) 3584-3601.

[56] S.Q. Yang, S.L. Xu, H.J. Huang, W. Zhang, X.G. Zhang, Prog. Chem. 20 (2008) 526-537.

[57] F.G. Li, Y.G. Bi, W.Y. Zhao, T.L. Zhang, Z.N. Zhou, L. Yang, Inorg. Chem. 54 (2015) 2050−2057.

[58] (a) V. Thottempudi, H. Gao, J. M. Shreeve, J. Am. Chem. Soc. 133 (2011) 6464-6471; (b) V. Thottempudi, J.M. Shreeve, J. Am. Chem. Soc. 133 (2011) 19982-19992; (c) K. Wang, D.A. Parrish, J.M. Shreeve, Chem. Eur. J. 17 (2011) 14485-14492; (d) K. Karaghiosoff, T.M. Klapötke, C.M. Sabaté, Eur. J. Inorg. Chem. 2009 (2009) 238-250; (e) T. Fendt, N. Fischer, T.M. Klapötke, J. Stierstorfer, Inorg. Chem. 2011, 50, 1447-1458; (f) T.M. Klapötke, D.G. Piercey, J. Stierstorfer, Chem. Eur. J. 2011, 17, 13068-13077; (g) T.M. Klapötke, D.G. Piercey, Inorg. Chem. 50 (2011) 2732-2734; (h) N. Fischer, D. Izsák, T.M. Klapötke, S. Rappenglueck, J. Stierstorfer, Chem. Eur. J. 18 (2012) 4051-4062; (i) T.M. Klapötke, F.A. Martin, J. Stierstorfer, Chem. Eur. J. 18 (2012) 1487-1501; (k) D. Fischer, N. Fischer, T.M. Klapötke, D.G. Piercey, J. Stierstorfer, Chem. Eur. J. 2013, 19, 4602-4613.

[59] (a) V. Thottempudi, F. Forohor, D.A. Parrish, J.M. Shreeve, Angew. Chem. Int. Ed. 51 (2012) 9881- 9885; (b) C. Qi, S.H. Li, Y.C. Li, Y. Wang, X.K. Chen, S.P. Pang, J. Mater. Chem. 21 (2011) 3221-3225; (c) V. Thottempudi, P. Yin, J.H. Zhang, D.A. Parrish, J.M. Shreeve, Chem. Eur. J. 20 (2014) 542-548.

[60] L.L. Zheng, H.X. Li, J.D. Leng, J. Wang, M.L. Tong, Eur. J. Inorg. Chem. (2008) 213-217.

[61] (a) J.P. Zhang, Y.Y. Lin, X.C. Huang, X.M. Chen, J. Am. Chem. Soc. 127 (2005) 5495-5506; (b) P.Q. Liao, D.D. Zhou, A.X. Zhu, L. Jiang, R.B. Lin, J.P. Zhang, X.M. Chen, J. Am. Chem. Soc. 134 (2012) 17380-17383; (c) J.P. Zhang, Y.B. Zhang, J.B. Lin, X.M. Chen, Chem. Rev. 112 (2012) 1001-1033.

[62] C. Qi, S.H. Li, Y.C. Li, Y. Wang, X.X. Zhao, S.P. Pang, Chem. Eur. J. 18 (2012) 16562-16570.

[63] (a) Y. Chuang, C. Liu, C. Sheu, W. Ho, G. Lee, C. Wang, Y. Wang, Inorg. Chem. 51 (2012) 4663-4671;

(b) Y. Chuang, W. Ho, C. Sheu, G. Lee, Y. Wang, Chem. Commun. 48 (2012) 10769-10771.

[64] (a) A. Gasco, R. Fruttero, G. Sorba, A. Di Stilo, R. Calvino, Pure Appl. Chem. 2004, 76, 973-981; (b) M. Boiani, H. Cerecetto, M.

Accepted Manuscript

ACCEPTED MANUSCRIPT

Gonzalez, M. Risso, C. Olea-Azar, O. Piro, E.E. Castellano, A.L. Cerain, O. Ezpeleta, A. Monge-Vega, Eur. J. Med. Chem. 36 (2001) 771-850; (c) C. Cena, S. Visentin, A. Di Stilo, D. Boschi, R. Fruttero, A. Gasco, Pharm. Res. 18 (2001) 157-165.

[65] (a) B.T. Federoff, Encyclopedia of Explosives and Related Items, Picatinny Arsenal, Dover, 1962; (b) Y. Oyumi, T.B. Brill, Combust. Flame. 65 (1986) 313-316; (c) B.M. Rice, J.J. Hare, J. Phys. Chem. A. 106 (2002) 1770-1783.

[66] (a) A.B. Sheremetev, J. Heterocycl. Chem. 32 (1995) 371-385; (b) T.S. Pivina, D.V. Sukhachev, A.V. Evtushenko, L.I. Khmelnitskii, Propel. Explos. Pyrotech. 20 (1995) 5-10; (c) A.B. Sheremetev, N.S. Aleksandrova, E.V. Mantseva, D.E. Dmitriev, Mendeleev Commun. 10 (2000) 67-69; (d) A.B. Sheremetev, E.V. Mantseva, D.E. Dmitriev, F.S. Sirovskii, Russ. Chem. Bull. Int. Ed. 51 (2002) 659-662; (e) A.M. Churakov, S.E. Semenov, S.L. Ioffe, Y.A. Strelenko, V.A. Tartakovskii, Mendeleev Commun. 5 (1995) 102-103.

[67] W. Zheng, J. Wang, X. Ren, Z. Chen, J. Tian, Y. Zhou, J. Hazard. Mater. 177 (2010) 738-742.

[68] C. Zhang, J. Mol. Struct. THEOCHEM. 765 (2006) 77-83.

[69] M. Friedrich, J.C. Gálvez-Ruiz, T.M. Klapötke, P. Mayer, B. Weber, J.J. Weigand, Inorg. Chem. 44 (2005) 8044-8052.

[70] S. Cudzilo, M. Nita, J. Hazard. Mater. 177 (2010) 146-149.

[71] B.D. Wu, J.G. Zhang, T.L. Zhang, L. Yang, Z.N. Zhou, Eur. J. Inorg. Chem. 2012 (2012) 1261-1268.

[72] S.W. Wang, L. Yang, J.L. Feng, B.D. Wu, J.G. Zhang, T.L. Zhang, Z.N. Zhou, Z. Anorg. Allg. Chem. 637 (2011) 2215-2222.

[73] M.A. Ilyushin, N.A. Petrova, I.V. Tselinsky. Chin. J. Energy. Mater. 1 (1993) 41-43.

[74] I.A. Ugryumov, M.A. Ilyushin, I.V. Tselinskii, A.S. Kozlov. Russ. J. Appl. Chem. 76 (2003) 439-441.

[75] M.A. Ilyushin, I.V. Tselinskiy, A.V. Smirnov, I.V. Shugalei. Cent. Eur. J. Energy Mater. 9 (2012) 3-16.

[76] L.Yang, B.D. Wu, T.L. Zhang, Z.H. Liu, J.G. Zhang, Propellants. Explos. Pyrotech. 35 (2010) 521-528.

[77] B.D. Wu, L. Yang, S.W. Wang, T.L. Zhang, J.G. Zhang, Z.N. Zhou, K.B. Yu, Z. Anorg. Allg. Chem. 637 (2011) 450-455.

[78] (a) J.P. Agrawal, High Energy Materials: Propellants, Explosives and Pyrotechnics; Wiley-VCH: Weinheim, Germany, 2010; (b) A.M. Astakhov, R.S. Stepanov, A.Y. Babushkin, Combus. Explos. Shock Waves. 34 (1998) 85-87; (c) B.J. Delley, J. Chem. Phys. 92 (1990) 508-517; (d) J.P. Perdew, K. Burke, M. Ernzerhof, Phys. Rev. Lett. 77 (1996) 3865-3868; (e) H.J. Monkhorst, J.D.Pack, Phys. Rev. B. 13 (1976) 5188-5192; (f) Zhu, S. G.; Wu, Y. C.; Zhang, W. Y.; Mu, J. Y. Propel. Explos. Pyrotech. 1997, 22, 317-320.

[79] Z. Tang , J.G. Zhang, Z.H. Liu, T.L. Zhang, L. Yang , X.J. Qiao, J. Mol. Struct. 1004 (2011) 8-12.

[80] (a) J.P. Agrawal, High Energy Materials: Propellants, Explosives and Pyrotechnics, Wiley-VCH, Weinhein, 2010; (b) A.M. Astakhov, R.S. Stepanov, A.Y. Babushkin, Combust. Explos. Shock Waves (Engl. Transl.) 34 (1998) 85-87.

[81] Z.H. Liu, T.L. Zhang, J.G. Zhang, S.Z. Wang, J. Hazard. Mater. 154 (2008) 832-838.

[82] (a) A.T. Nielsen, A.P. Chafin, S.L. Christian, DW. Moore, M.P. Nadler, R.A. Nissan, D.J. Vanderah, Tetrahedron. 54 (1998)11793-11812; (b) A.T. Nielsen, R.A. Nissan, D.J. Vanderah, J. Org. Chem. 55 (1990) 1459-1466; (c) Y. Wang, C. Qi, J. Song, X.

Accepted Manuscript

ACCEPTED MANUSCRIPT

Zhao, C. Sun, S. Pang, J. Mol. Model. 19 (2013) 1079-1087; (d) C. Sun, X. Zhao, Y. Li, S. Pang, Chin. Chem. Lett. 21 (2010) 572-575;

(e) R. Duddu, P.R. Dave, R. Damavarapu, R. Surapaneni, R. Gilardi, D. Parrish, Synth. Commun. 38 (2008) 767-774.

Accepted Manuscript

ACCEPTED MANUSCRIPT

Figure Captions:

Scheme 1 Triazole and its derivatives.

Scheme 2 Tetrazole and its derivatives.

Scheme 3 Triazine, tetrazine and their derivatives.

Scheme 4 Hydrazine and its derivatives.

Scheme 5 Furazan (furoxan) and its derivatives.

Scheme 6 Energetic moities.

Figure 1. The zigzag chain of **1**.

Figure 2. An infinite one-dimensional coordination array polymer built from centroasymmetric mononuclear [Ag(MHT)(H_2O)] units and MHT bridges in **2**.

Figure 3. Synthesis and 1D structure of $\{[Cu_n(ATZ)_3](ClO_4)_2\}_n$.

Figure 4. 1D chain structure of **4** along the Zn···Zn axis, surrounding with PA molecules in the external zone.

Figure 5. The five-member and six-member rings give linear chains along *a* axis, thus, a 1-D coordination polymer is formed, surrounding with NO_3^- anions in the external zone in **6**.

Figure 6. A drawing of the 1D loop chain in **7**, surrounding with ClO_4^- anions in the external zone.

Figure 7. One-dimensional chain structure of **8** viewed along the *a* axis of the unit cell.

Figure 8. The one-dimensional chain structure along *a*-axis in $[Cd(en)(N_3)_2]_n$ and octahedral coordination structure of Cd(II).

Figure 9. A one-dimensional chain runs along *a* axis of the unit cell with alternating six-membered Zn–N4–Zn rings in **10**.

Figure 10. Crystal structure of NHP, surrounding with ClO_4^- anions in the external zone.

Figure 11. Structure of NHN, surrounding with NO_3^- anions in the external zone.

Chart 1. Energy of detonation for DFT-optimized structures ($\Delta E_{DFT,\ det}$) *vs* estimated heat of detonation (ΔH_{det}) from literature for 11 highly explosive materials (Values are from ref 78a for explosives **1**−**9** and ref 78b for explosives **10** and **11**. MF, mercury fulminate; ONC, octanitrocubane; other abbreviations are common explosive names.); (b) Bar diagram representation of the literature ΔH_{det} values for the 11 highly explosive

ACCEPTED MANUSCRIPT

materials along with the predicted ΔH_{det} for NHN, CHP, and NHP using the linear correlation developed in Chart 1a (a Also indicated are the error margins for the predicted values at the 95% confidence level. Both mass-density (kcal·g^{-1}) and volume-density (kcal·cm^{-3}) of the ΔH_{det} are indicated, and the heats are arranged in increasing order of volume-density.)

Figure 12. Six-coordinated Cu^{II} ions linked through the azido groups with μ-1,1,3 coordination mode to obtain 1D line in **14**.

Figure 13. The moleculars tructures of **15**. the slightly distorted-octahedral Cu1 cations are bridged azido groups with μ-1,1 bridging ligand and μ-1,1,3 coordination modes to obtain a 2D network.

Figure 14. The two zigzag chains linked by azido ligands are vertical to each other, and a novel two-dimensional rectangular-grid-like layer parallel to ab-plane of unit cell is formed in **16**.

Figure 15. The six-coordinated Cd(II) cations are inter linked by μ-Cl ligands and HATr ligands to generate a 2D framework in **17**.

Figure 16. 2D network with MHT anions as bridging ligands in **18**.

Figure 17. Partial packing diagram of CHHP showing the sheet structure parallel to *bc* plane.

Figure 18. Partial packing diagram of a ZnHHP sheet showing the ladder motif. In both graphics, perchlorate anions and cocrystallized water have been omitted for clarity.

Chart 2. Bar chart representation of the literature ΔH_{det} values for eleven common explosive materials.[64a,64b] Previously reported values for CHP, NHP, and NHN, along with the predicted ΔH_{det} values for CHHP and ZnHHP are also shown. Error bars correspond to the 95% statistical-confidence level for these values.

Figure 19. Binuclear polymers with Pb⋯Pb 4.503 Å are bridged water O1 to generate 2D sheet viewed along *a* axis in **21**.

Figure 20. The 2D layer is formed based on the coordination of O with Pb(II) ion at the axial position in **22**.

Figure 21. The 2D layer, in which the adjacent Pb(II) centers are linked by the bridging H_2tztr ligand in two different directions to form a slightly distorted 2D (4, 4) sheet in **23**.

Figure 22. The 2D layer-like structure is constructed by the interlinkages between Cu(I) ions and

ACCEPTED MANUSCRIPT

H_2tztr ligands in **24**.

Chart 3. Bar chart representation of the previously reported ΔH_{det} values for the common explosive materials, including CL-20 and ONC. Previously reported values for energetic MOFs (ZnHHP, CHHP, CHP, NHP, ATRZ-1, and ATRZ-2), along with the predicted ΔH_{det} value for **24** and **37** are also shown.

Figure 23. In isostructural **25** and **26**, the chiral chain connects two adjacent opposite chiral ones byμ_2-κN3:κN4 tetrazolate groups to form an achiral 2D framework parallel to *bc* plane.

Figure 24. Polyhedral view of the 1D chain along *a*-axis and 2D plane along *c*-axis in **27**. [SrO6]: green triple prism; [SrO6N3]: red three-capped triangle prism. All H atoms are omitted for clarity.

Figure 25. The dimeric units of Cd_2N_2, $Cd_2(NNN)_2$, $Cd_2(NN)_2$ bridged through double μ-1, 1 azide bridges, μ-1, 3 azide bridges and bidentate bridging hydrazine ligands, respectively, to generate a 3D network structure in **29**.

Figure 26. Interweaving of left/righthanded helical chains leads to an achiral 3D framework with void helical channels which have an opening with a maximum diameter of 5.90 Å (atom-to-atom distance) with a screw axis along *c* axis in **30**.

Figure 27. The 3D porous MOF of **31** depicted along the crystallographic *a* axis and the pores along *a* axis are filled with nitrate anions.

Figure 28. The 3D porous MOF of **32** depicted along the crystallographic *a* axis, and the pores along *a* axis are filled with nitrate anions.

Chart 4. Bar chart respresentation of the literature ΔH_{det} values for the common explosive materials including hexanitrohexaazaisowutzitane (CL-20), and octanitrocubane (ONC). Previously reported values for energetic MOFs (NHN, CHHP, ZnHHP, CHP, and NHP), along with the predicted ΔH_{det} values for **31** (ATRZ-1) and **32** (ATRZ-2) are also shown. Error bars correspond to the 95% statistical-confidence level for these values.

Figure 29. 3D mixed valence CoIII–CoII energetic MOF with channels incorporating the latticed water molecules in **33**.

Chart 5. Bar chart representation of the literature ΔH_{det} values for the common explosive materials, including CL-20 and ONC. Previously reported values for energetic MOFs (ZnHHP, CHHP, CHP, NHP, ATRZ-1, and ATRZ-2), along with the predicted ΔH_{det}

ACCEPTED MANUSCRIPT

value for 2 are also shown. Error bars correspond to the 95% statistical-confidence level for these values.

Figure 30. 3D network in **35** extended based on the 1D $Na_2(azole)_2$-SBU beetle-like chains .

Chart 6. Bar chart representation of the literature ΔH_{det} values for the common explosive materials including Previously reported values for energetic MOFs (HMX, RDX, TNT, ATRZ-1, ATRZ-2, CHP, NHP, CHHP, and ZnHHP), along with the predictedΔH_{det} value for **35** is also shown. Error bars correspond to the 95% statistical-confidence level for these values.

Figure 31. 3D porous structure of **36** of which the pores are filled with lattice water molecules.

Figure 32. Adjacent Cu(II) ions are linked by an azide bridge in m-1,1 (or end-on, EO) mode and a carboxylate bridge in *syn–syn* mode, yielding a formal 1D chain along the crystallographic a direction. Furthermore, nitro groups on the intrachain 3,5-DNBA molecules are connected to Cu(II) ions from other chains, forming a three-dimensional network structure in **37**.

Table 1 Physicochemical properties of **1**–**37** and some energetic materials.

Accepted Manuscript

ACCEPTED MANUSCRIPT

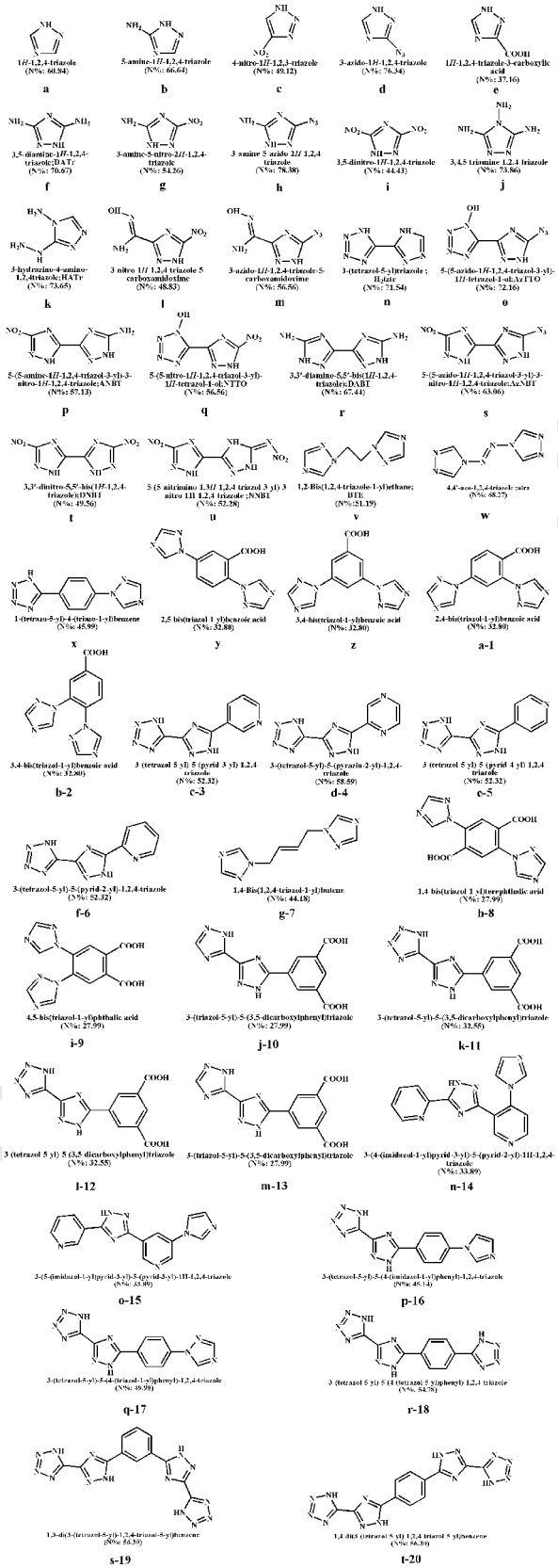

Scheme 1 Triazole and its derivatives.

ACCEPTED MANUSCRIPT

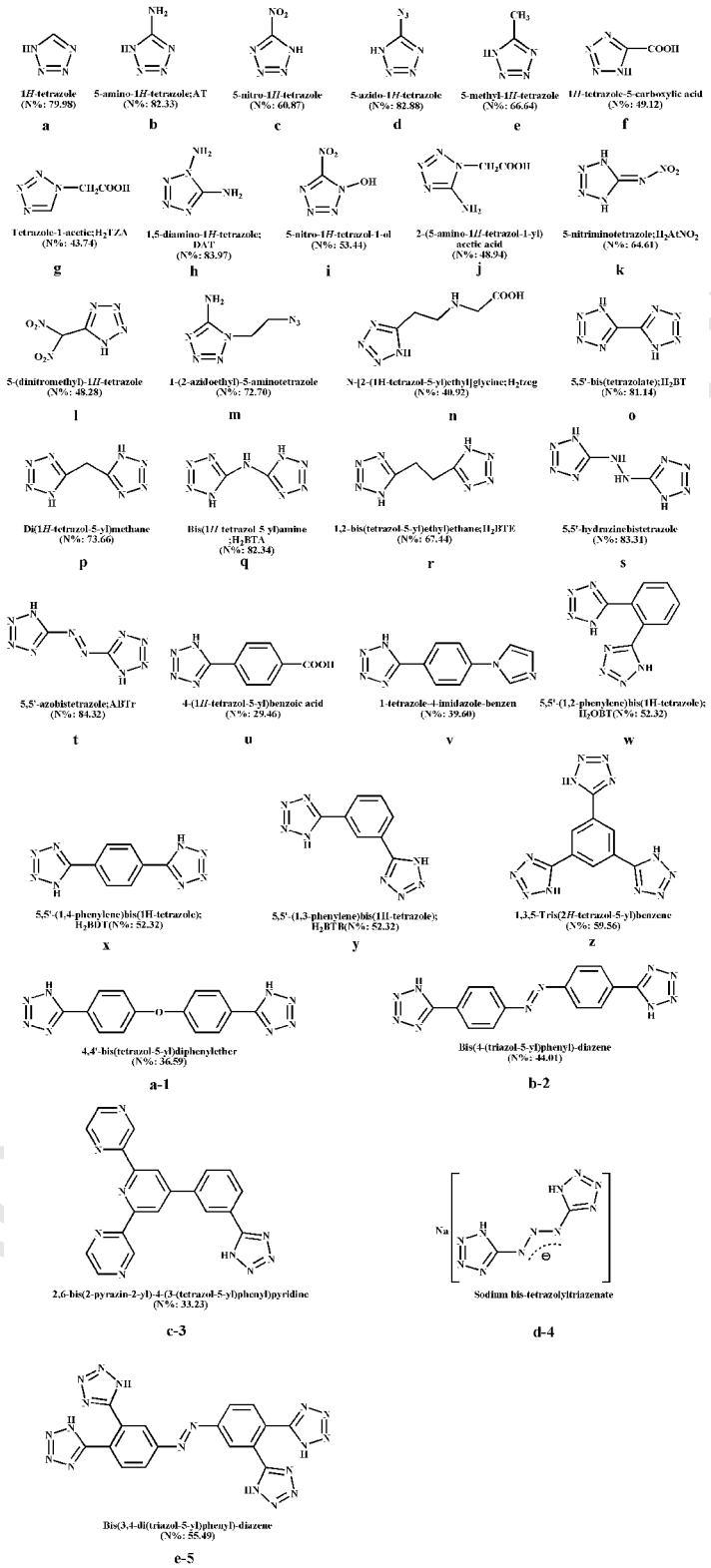

Scheme 2 Tetrazole and its derivatives.

ACCEPTED MANUSCRIPT

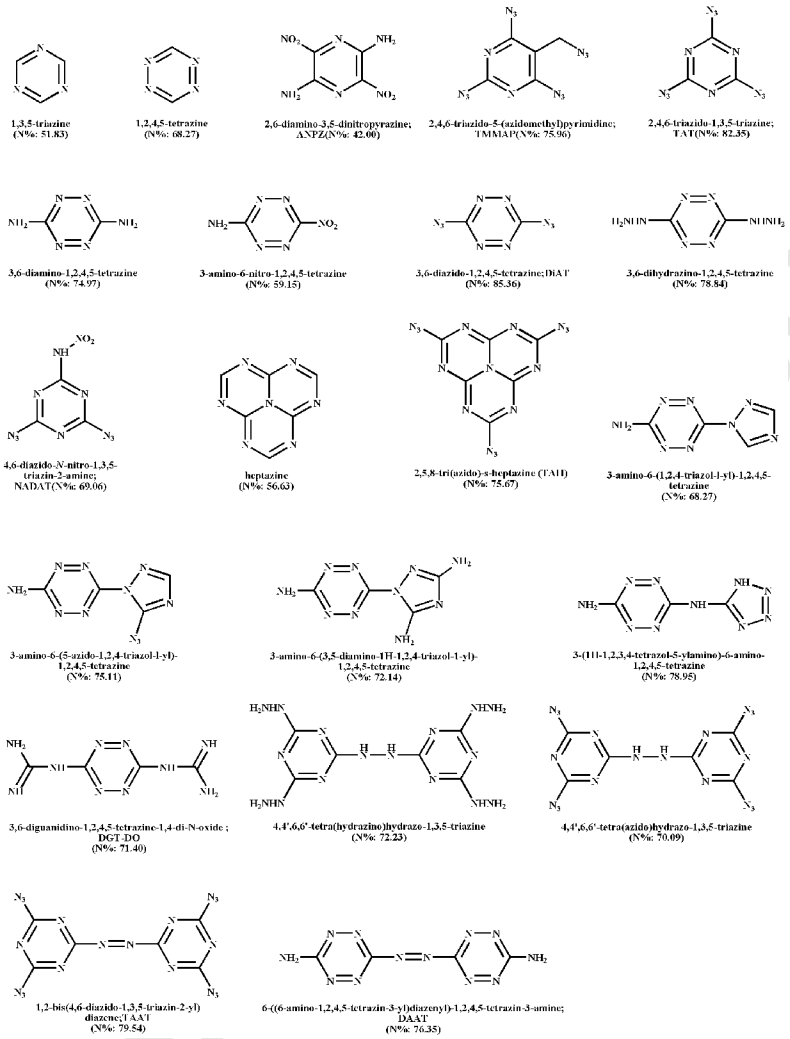

Scheme 3 Triazine, tetrazine and their derivatives.

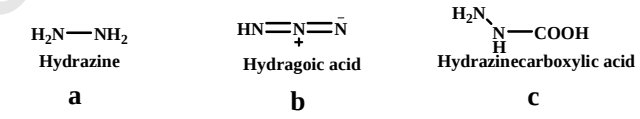

Scheme 4 Hydrazine and its derivatives.

ACCEPTED MANUSCRIPT

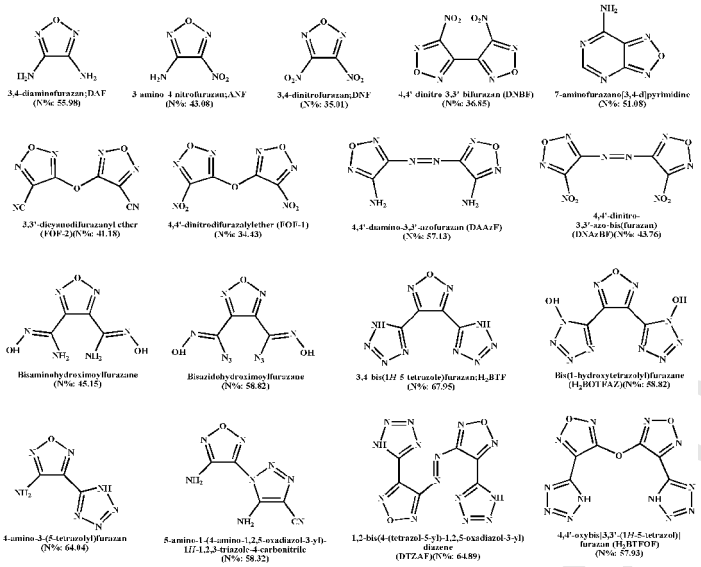

Scheme 5 Furazan (furoxan) and its derivatives.

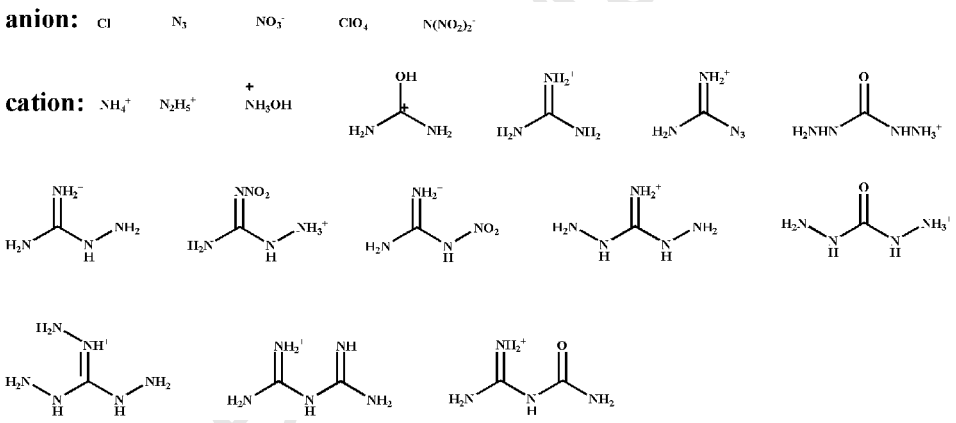

Scheme 6 Energetic moities.

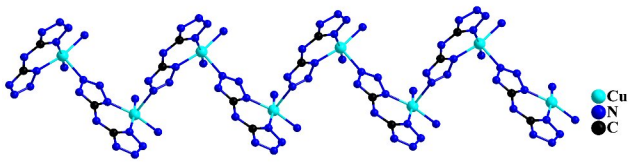

Figure 1. The zigzag chain of **1**.

ACCEPTED MANUSCRIPT

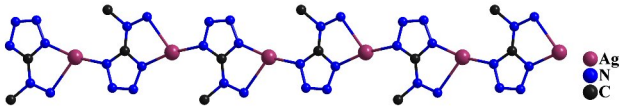

Figure 2. An infinite one-dimensional coordination array polymer built from centroasymmetric mononuclear [Ag(MHT)(H_2O)] units and MHT bridges in **2**.

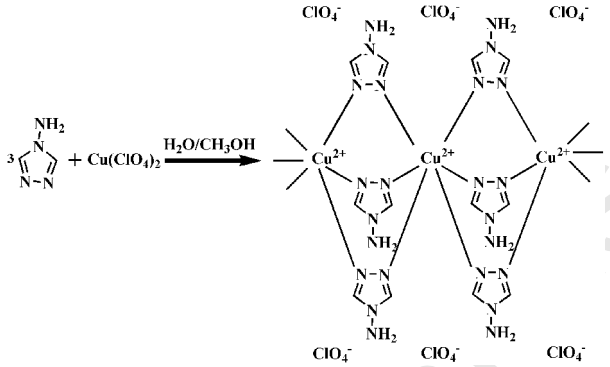

Figure 3. Synthesis and 1D structure of $\{[Cu_n(ATZ)_3](ClO_4)_2\}_n$.

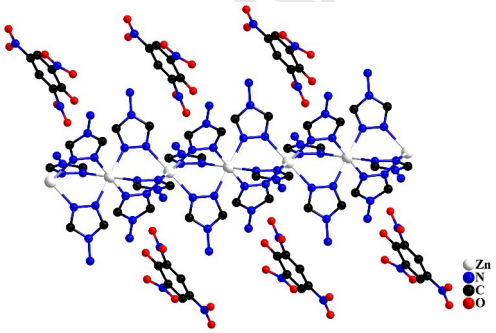

Figure 4. 1D chain structure of **4** along the Zn···Zn axis, surrounding with PA molecules in the external zone.

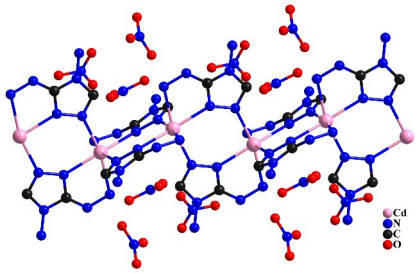

Figure 5. The five-member and six-member rings give linear chains along *a* axis, thus, a 1-D coordination polymer is formed, surrounding with NO_3^- anions in the external zone in **6**.

ACCEPTED MANUSCRIPT

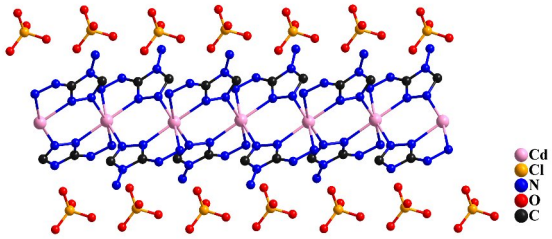

Figure 6. A drawing of the 1D loop chain in **7**, surrounding with ClO_4^- anions in the external zone.

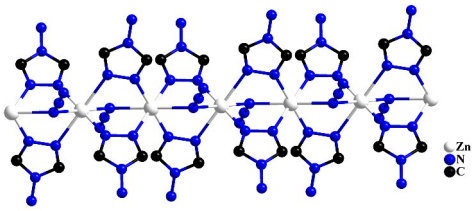

Figure 7. One-dimensional chain structure of **8** viewed along the *a* axis of the unit cell.

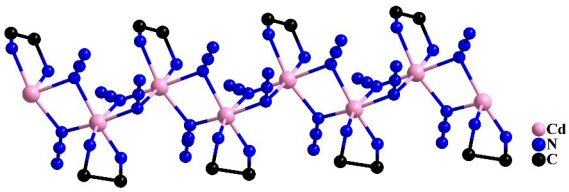

Figure 8. The one-dimensional chain structure along *a* axis in $[Cd(en)(N_3)_2]_n$ and octahedral coordination structure of Cd(II).

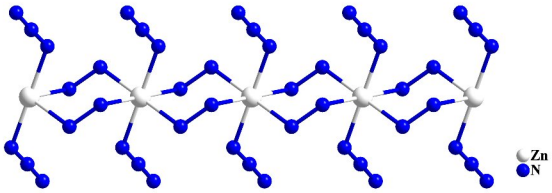

Figure 9. A one-dimensional chain runs along *a* axis of the unit cell with alternating six-membered Zn–N4–Zn ring in **10**.

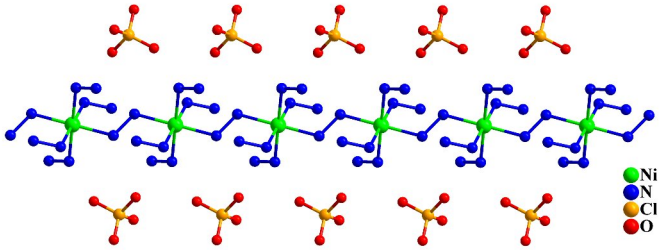

Figure 10. Crystal structure of NHP, surrounding with ClO_4^- anions in the external zone.

ACCEPTED MANUSCRIPT

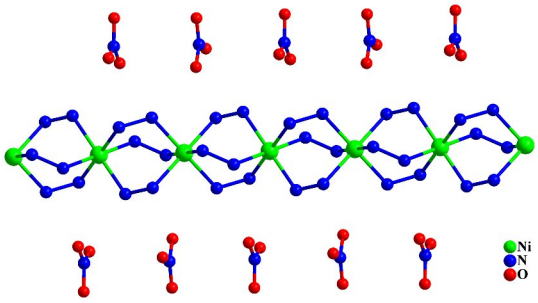

Figure 11. Structure of NHN, surrounding with NO_3^- anions in the external zone.

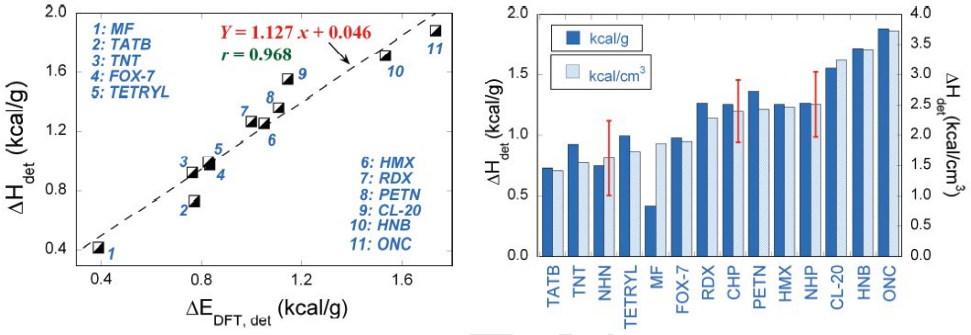

a **b**

Chart 1. Energy of detonation for DFT-optimized structures ($\Delta E_{DFT,\ det}$) *vs* estimated heat of detonation (ΔH_{det}) from literature for 11 highly explosive materials (Values are from ref 78a for explosives **1**–**9** and ref 78b for explosives **10** and **11**. MF, mercury fulminate; ONC, octanitrocubane; other abbreviations are common explosive names.); (b) Bar diagram representation of the literature ΔH_{det} values for the 11 highly explosive materials along with the predicted ΔH_{det} for NHN, CHP, and NHP using the linear correlation developed in Chart 1a (a Also indicated are the error margins for the predicted values at the 95% confidence level. Both mass-density (kcal•g^{-1}) and volume-density (kcal•cm^{-3}) of the ΔH_{det} are indicated, and the heats are arranged in increasing order of volume-density.)

ACCEPTED MANUSCRIPT

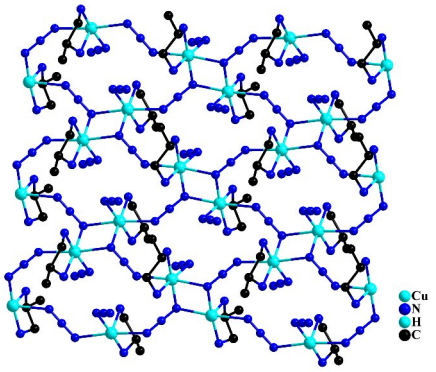

Figure 12. Six-coordinated Cu^{II} ions linked through the azido groups with μ-1,1,3 coordination mode to obtain 1D line in **14**.

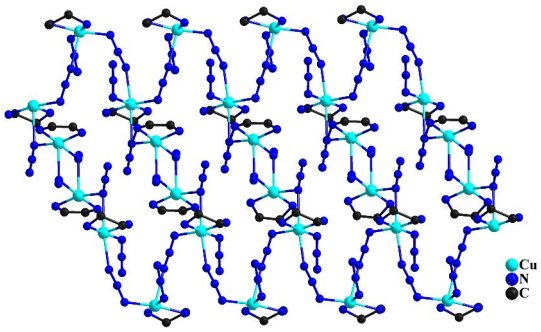

Figure 13. The moleculars tructures of **15**. the slightly distorted-octahedral Cu1 cations are bridged azido groups with μ-1,1 bridging ligand and μ-1,1,3 coordination modes to obtain a 2D network.

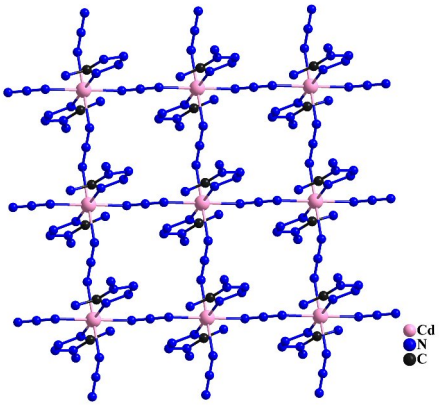

Figure 14. The two zigzag chains linked by azido ligands are vertical to each other, and a novel two-dimensional rectangular-grid-like layer parallel to ab-plane of unit cell is formed in **16**.

ACCEPTED MANUSCRIPT

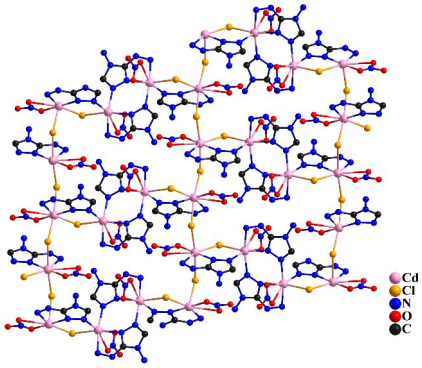

Figure 15. The six-coordinated Cd(II) cations are inter linked by μ-Cl ligands and HATr ligands to generate a 2D framework in **17**.

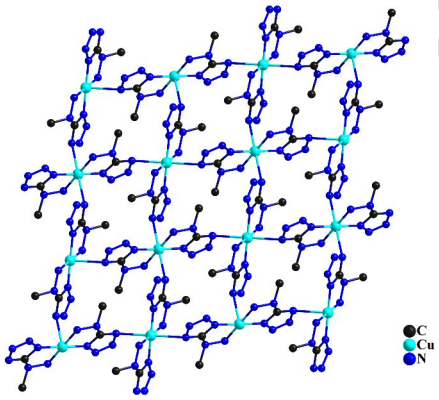

Figure 16. 2D network with MHT anions as bridging ligands in **18**.

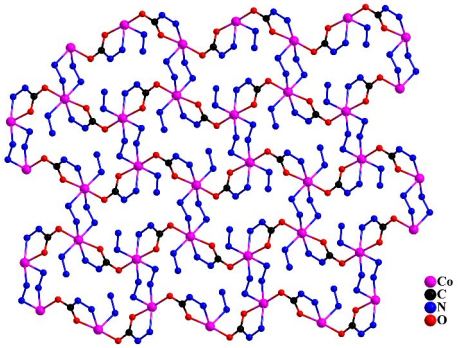

Figure 17. Partial packing diagram of CHHP showing the sheet structure parallel to *bc* plane.

ACCEPTED MANUSCRIPT

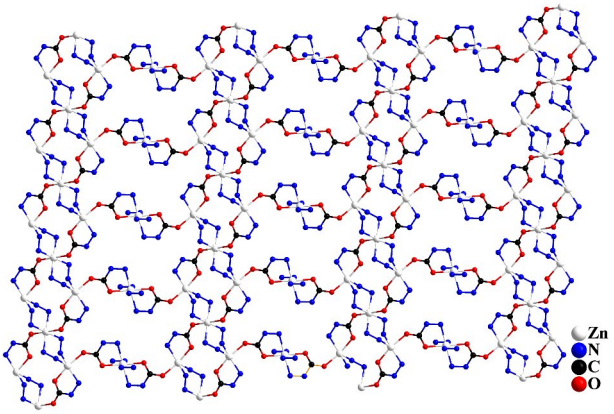

Figure 18. Partial packing diagram of a ZnHHP sheet showing the ladder motif. In both graphics, perchlorate anions and cocrystallized water have been omitted for clarity.

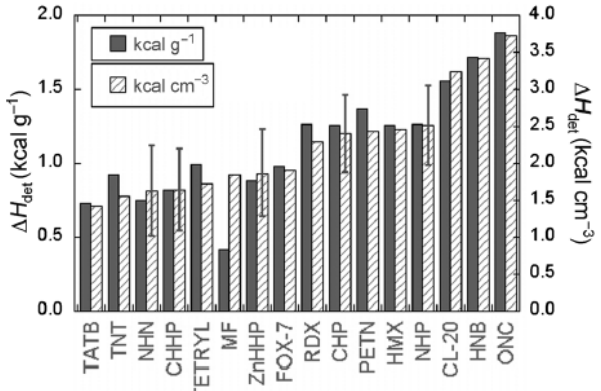

Chart 2. Bar chart representation of the literature ΔH_{det} values for eleven common explosive materials.[64a,64b] Previously reported values for CHP, NHP, and NHN, along with the predicted ΔH_{det} values for CHHP and ZnHHP are also shown. Error bars correspond to the 95% statistical-confidence level for these values.

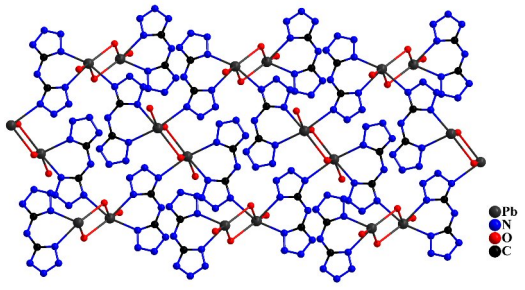

Figure 19. Binuclear polymers with Pb···Pb 4.503 Å are bridged water O1 to generate 2D sheet viewed along *a* axis in **21**.

ACCEPTED MANUSCRIPT

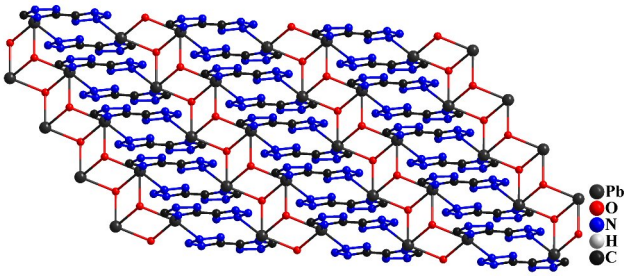

Figure 20. The 2D layer is formed based on the coordination of O with Pb(II) ion at the axial position in **22**.

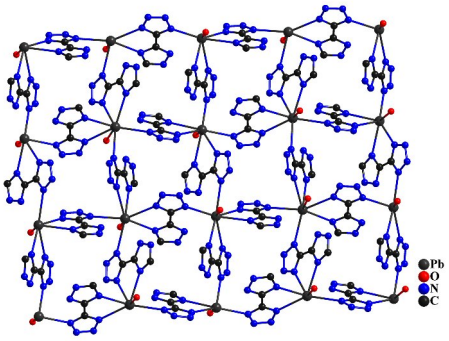

Figure 21. The 2D layer, in which the adjacent Pb(II) centers are linked by the bridging H_2tztr ligand in two different directions to form a slightly distorted 2D (4, 4) sheet in **23**.

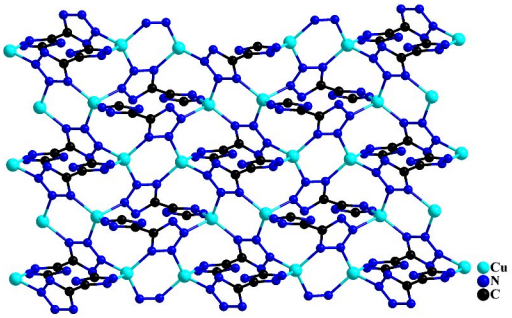

Figure 22. The 2D layer-like structure is constructed by the interlinkages between Cu(I) ions and H_2tztr ligands in **24**.

ACCEPTED MANUSCRIPT

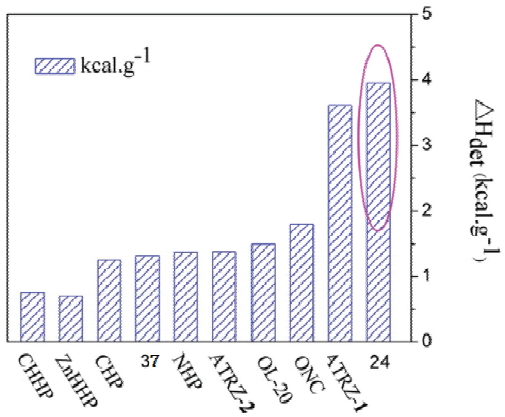

Chart 3. Bar chart representation of the previously reported ΔH_{det} values for the common explosive materials, including CL-20 and ONC. Previously reported values for energetic MOFs (ZnHHP, CHHP, CHP, NHP, ATRZ-1, and ATRZ-2), along with the predicted ΔH_{det} value for **24** and **37** are also shown.

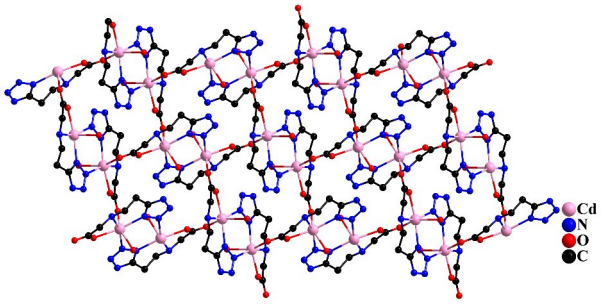

Figure 23. In isostructural **25** and **26**, the chiral chain connects two adjacent opposite chiral ones byμ_2-κN3:κN4 tetrazolate groups to form an achiral 2D framework parallel to *bc* plane.

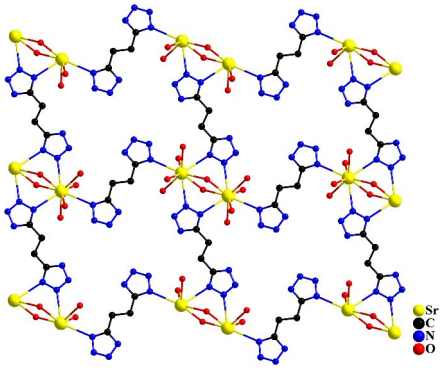

Figure 24. Polyhedral view of the 1D chain along *a*-axis and 2D plane along *c*-axis in **27**. [SrO6]: green triple prism;[SrO6N3]: red three-capped triangle prism. All H atoms are omitted for clarity.

ACCEPTED MANUSCRIPT

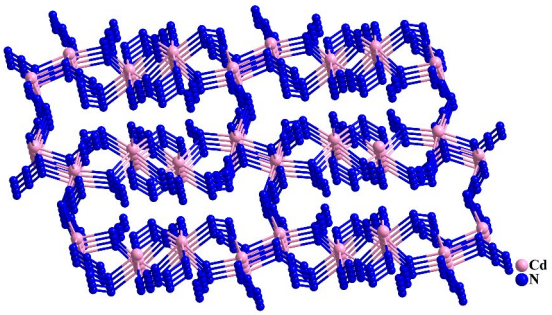

Figure 25. The dimeric units of Cd_2N_2, $Cd_2(NNN)_2$, $Cd_2(NN)_2$ bridged through double μ-1, 1 azide bridges, μ-1, 3 azide bridges and bidentate bridging hydrazine ligands, respectively, to generate a 3D network structure in **29**.

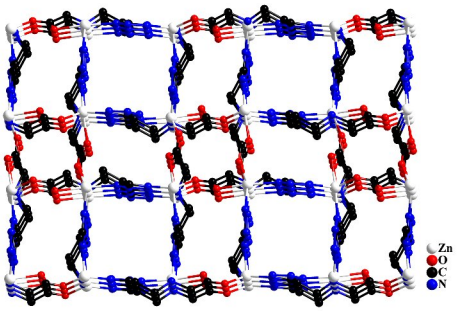

Figure 26. Interweaving of left/righthanded helical chains leads to an achiral 3D framework with void helical channels which have an opening with a maximum diameter of 5.90 Å (atom-to-atom distance) with a screw axis along *c* axis in **30**.

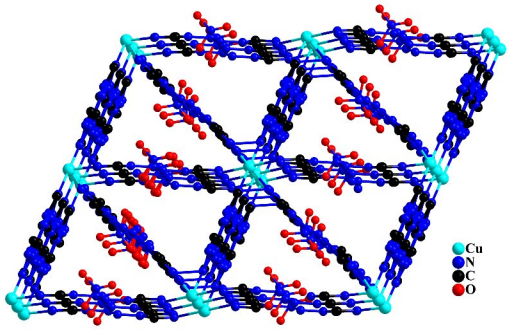

Figure 27. The 3D porous MOF of **31** depicted along the crystallographic *a* axis and the pores along *a* axis are filled with nitrate anions.

ACCEPTED MANUSCRIPT

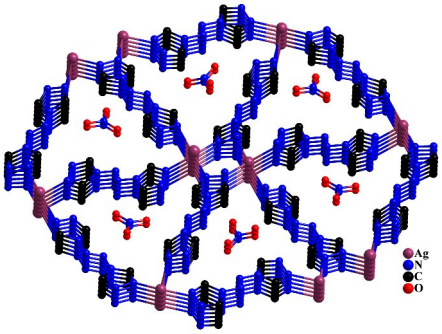

Figure 28. The 3D porous MOF of **32** depicted along the crystallographic *a* axis, and the pores along *a* axis are filled with nitrate anions.

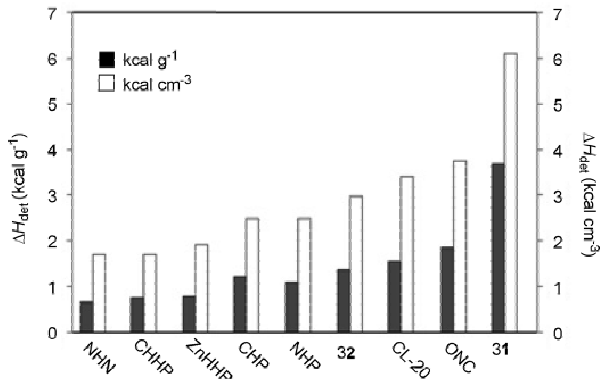

Chart 4. Bar chart respresentation of the literature ΔH_{det} values for the common explosive materials including hexanitrohexaazaisowutzitane (CL-20), and octanitrocubane (ONC). Previously reported values for energetic MOFs (NHN, CHHP, ZnHHP, CHP, and NHP), along with the predicted ΔH_{det} values for **31** (ATRZ-1) and **32** (ATRZ-2) are also shown. Error bars correspond to the 95% statistical-confidence level for these values.

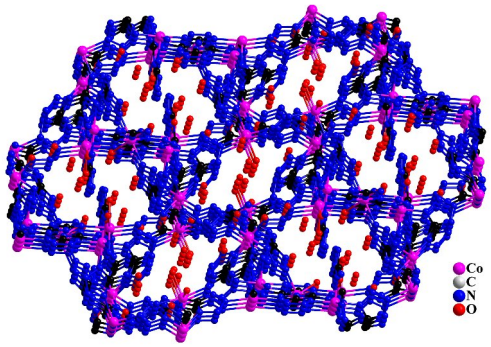

Figure 29. 3D mixed valence CoIII–CoII energetic MOF with channels incorporating the latticed water molecules

ACCEPTED MANUSCRIPT

in **33**.

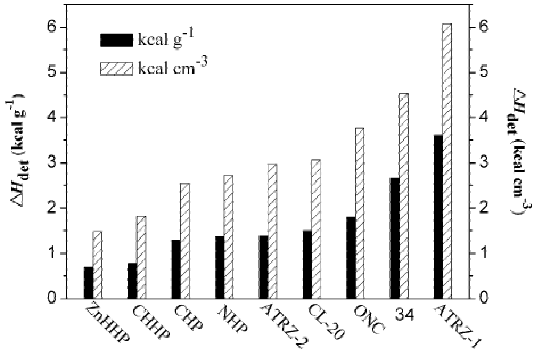

Chart 5. Bar chart representation of the literature ΔH_{det} values for the common explosive materials, including CL-20 and ONC. Previously reported values for energetic MOFs (ZnHHP, CHHP, CHP, NHP, ATRZ-1, and ATRZ-2), along with the predicted ΔH_{det} value for 2 are also shown. Error bars correspond to the 95% statistical-confidence level for these values.

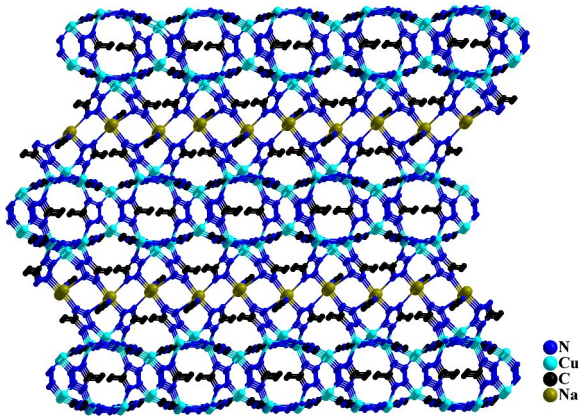

Figure 30. 3D network in **35** extended based on the 1D $Na_2(azole)_2$-SBU beetle-like chains.

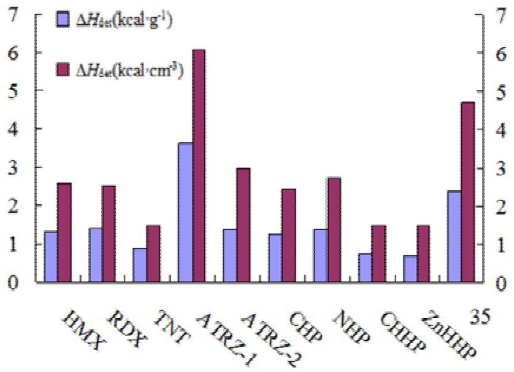

ACCEPTED MANUSCRIPT

Chart 6. Bar chart representation of the literature ΔH_{det} values for the common explosive materials including Previously reported values for energetic MOFs (HMX, RDX, TNT, ATRZ-1, ATRZ-2, CHP, NHP, CHHP, and ZnHHP), along with the predictedΔH_{det} value for **35** is also shown. Error bars correspond to the 95% statistical-confidence level for these values.

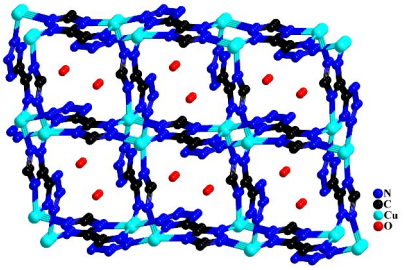

Figure 31. 3D porous structure of **36** of which the pores are filled with lattice water molecules.

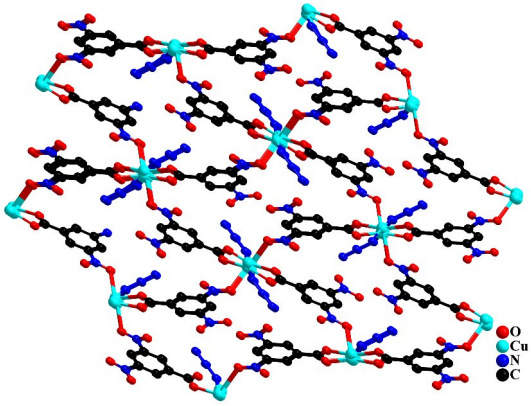

Figure 32. Adjacent Cu(II) ions are linked by an azide bridge in m-1,1 (or end-on, EO) mode and a carboxylate bridge in *syn–syn* mode, yielding a formal 1D chain along the crystallographic a direction. Furthermore, nitro groups on the intrachain 3,5-DNBA molecules are connected to Cu(II) ions from other chains, forming a three-dimensional network structure in **37**.

ACCEPTED MANUSCRIPT

Table 1 Physicochemical properties of **1**–**37** and some energetic materials.

MOFs	Dimension	N%[a] (MOF)	Configuration	Ligand	Formula	T_{dec} [b] (℃)	Ω[c] (%)	IS (J) [d] FS (N)[e] EDS (J)[f]	ρ[g] ($g\cdot cm^{-3}$)	$\Delta_f H_m^\theta$ [h] ($kJ\cdot mol^{-1}$)	$\Delta_c H_m^\theta$ [i] ($kJ\cdot mol^{-1}$)	ΔE_{det} [j] ($kcal\cdot g^{-1}$)	ΔH_{det} [k] ($kcal\cdot g^{-1}$)	ΔH_{det} [l] ($kcal\cdot cm^{-3}$)	D[m] ($km\cdot s^{-1}$)	P[n] (GPa)
1	1	62.0	square pyramidal	N,N-bis(1H-tetrazole-5-yl)-amine,H_2bta	$[Cu(bta)(NH_3)_2\cdot H_2O]_n$	250	-48.3	>40,>360,-	1.9982	87.8	-555.5	-	-	-	-	-
2	1	35.17	planar	5-(1-methylhydrazinyl) tetrazole, MHT	$\{[Ag(MHT)]\cdot H_2O\}_n$	200	-50.2	>40,-,-	2.465	-263	1539	-	-	-	-	-
3	1	32.66	-	4-amino-1,2,4-triazole, ATZ	$\{[Cu(ATZ)](ClO_4)_2\}_n$	>250	-34.2	1,8.8,-	1.4	-	-	-	-	-	6.5	-
4	1	30.89	distorted octahedral	4-amino-1,2,4-triazole, ATZ; picrate, PA	$\{Zn(ATZ)_3](PA)_2\cdot 2.5H_2O\}_n$	276.3	-60.57	27.8,-,-	1.757	-1150.1	-9278.13	-	-	-	-	-
5	1	46.12	octahedral	3-Hydrazino-4-amino-1,2,4-triazole, HATr	$[Mn_2(HATr)_4(NO_3)_4\cdot 2H_2O]_n$	260	-33.86	-,-,-	1.864	-1002.35	-7211.9	-	-	-	-	-
6	1	41.40	octahedral	3-Hydrazino-4-amino-1,2,4-triazole, HATr	$[Cd_2(HATr)_4(NO_3)_4\cdot H_2O]_n$	295	-30.40	-,-,-	2.021	-457.27	-6953.7	-	-	-	-	-
7	1	31.12	octahedral	3-Hydrazino-4-amino-1,2,4-triazole, HATr	$[Cd(HATr)_2(ClO_4)_2]_n$	322.5	-20.76	-,-,-	2.240	-	-	-	-	-	-	-
8	1	61.7	octahedral	4-amino-1,2,4-triazole, ATZ	$[Zn_3(ATZ)_6(N_3)_6]_n$	136.85	-60.45	>40,-,-	1.824							
9	1	43.67	distorted octahedral	Ethylenediamine,en; azide, N_3	$[Cd(en)(N_3)_2]_n$	149.85	-49.89	3.4,-,-	2.090	-	-	-	-	-	-	-
10	1	65.60	distorted octahedral	Hydrazine, N_2H_4; azide, N_3	$[Zn(N_2H_4)_2(N_3)_2]_n$	200.85	-29.97	28.5,-,-	2.083	-	1163.74	-	-	-	-	-

ACCEPTED MANUSCRIPT

11	1	33.49	octahedral	Hydrazine, N_2H_4	$[Ni(N_2H_4)_5(ClO_4)_2]_n$	220	-11.48	-,-,-	1.983	-	-	1.174	1.370	2.72	9.2	36.8
12	1	33.49	octahedral	Hydrazine, N_2H_4	$[Co(N_2H_4)_5(ClO_4)_2]_n$	194	-11.48	0.5,-,-	1.948	-	-	1.068	1.250	2.44	8.225	31.73
13	1	40.14	octahedral	Hydrazine, N_2H_4	$[Ni(N_2H_4)_3(NO_3)_2]_n$	-	-5.73	-,-,-	2.156	-	-	0.859	1.014	2.16	7.3	20.2
14	2	50.54	distorted octahedral	1,2-diaminopropane, pn; azide, N_3	$[Cu(pn)(N_3)_2]_n$	215.7	-86.6	2.55,-,-	1.762	-2320.76	-982.44					
15	2	53.95	distorted octahedral	Ethylenediamine,en; azide, N_3	$[Cu_2(en)_2(N_3)_4]_n$	201.8	-69.33	7.84,-,-	1.928	-1330.34	-2840.46	-	-	-	-	-
16	2	63.42	octahedral	1,5-diaminotetrazole, DAT; azide, N_3	$[Cd(DAT)_2(N_3)_2]_n$	208	-32.27	-,-,-	2.144	-	-	-	-	-	-	-
17	2	30.26	octahedral	3-Hydrazino-4-amino-1,2,4-triazole, HATr	$[Cd2(NO_3)_2Cl_2(HATr)_2]_n$	224.85	-24.69	-,-,-	2.470	-	-	-	-	-	-	-
18	2	58.01	octahedral	5-(1-methylhydrazinyl) tetrazole, MHT	$[Cu(MHT)_2]_n$	200	-77.30	>40,-,-	2.031	93	-3253	-	-	-	-	-
19	2	23.58	distorted octahedral	Hydrazine carboxylate, $N_2H_3CO_2$; hydrazine, N_2H_4	$\{[Co_2(N_2H_4)_4(N_2H_3CO_2)_2]\cdot 2ClO_4\cdot H_2O\}_n$	231	-13.05	0.8,-,-	2.000			0.625	0.750	1.5	6.205	17.96
20	2	23.61	octahedral	Hydrazine carboxylate, $N_2H_3CO_2$; hydrazine, N_2H_4	$\{[Zn_2(N_2H_4)_3(N_2H_3CO_2)_2]\cdot 2ClO_4\cdot H_2O\}_n$	293	-49.99	-,-,-	2.117			0.580	0.7	1.482	7.016	23.58
21	2	31.97	Square pyramidal	N,N-bis[1(2)H-tetrazol-5-yl]amin, H_2bta	$[Pb(bta)(H_2O)_2]_n$	160	-18.26	-,-,-	3.214	-	-	-	-	-	-	-
22	2	39.40	distorted pentagonal bipyramid	3-(1H-tetrazol-5-yl)-1H-triazole, H_2tztr	$[Pb(Htztr)2(H2O)]_n$	340	-45.03	>40,>360,-	2.519	665.47	-4103.52	1.165	1.359	3.423	7.715	31.57

ACCEPTED MANUSCRIPT

23	2	27.20	distorted pentagonal pyramid	3-(1H-tetrazol-5-yl)-1H -triazole, H_2tztr	$[Pb(H_2tztr)(O)]_n$	318	-28.86	>40,>360,-	3.511	889.62	-2718.39	0.185	0.255	0.895	8.122	40.12
24	2	49.08	distorted tetrahedral	3-(1H-tetrazol-5-yl)-1H -triazole, H_2tztr	$[Cu(Htztr)]_n$	355	-56.09	32,>360, 24.75	2.435	-	-	3.4714	3.9582	9.6382	10.40	56.48
25	2	23.38	distorted octahedral	N-[2-(1H-tetrazol-5-yl) ethyl]glycine, H_2tzeg	$[Cd(tzeg)(H_2O)]_n$	275	-66.8	-,-,-	2.242	-559.28	-2953.76	-	-	-	-	-
26	2	27.93	elongated octahedral	N-[2-(1H-tetrazol-5-yl) ethyl]glycine, H_2tzeg	$[Cu(tzeg)(H_2O)]_n$	350	-79.8	-,-,-	2.005	-508.19	-2900.71	-	-	-	-	-
27	2	32.78	three-capped triangle prism	1,2-bis(tetrazol-5-yl)eth ane, H_2BTE	$[Sr(BTE)(H_2O)_5]_n$	>350	-51.48	-,-,-	1.958	-	-	-	-	-	-	-
28	2	28.62	three-capped triangle prism	1,2-bis(tetrazol-5-yl)eth ane, H_2BTE	$[Ba(BTE)(H_2O)_5]_n$	>350	-44.95	-,-,-	2.098	-	-	-	-	-	-	-
29	3	49.01	distorted octahedral	Hydrazine, N_2H_4; azide, N_3	$[Cd_2(N_2H_4)_2(N_3)_4]_n$	151	-21.0	>40,-,-	2.638	-	-	-	-	-	-	-
30	3	29.86	distorted trigonal bipyramidal polyhedron	N-[2-(1H-tetrazol-5-yl) ethyl]glycine, H_2tzeg	$[Zn(tzeg)]_n$	425	-85.3	-,-,-	1.882	-491.78	-2823.74	-	-	-	-	-
31	3	53.35	octahedron	4,4'-azo-1,2,4-triazole, atrz	$[Cu(atrz)_3(NO_3)_2]_n$	243	-58.83	22.5,-,-	1.68	-	-	3.169	3.618	6.078	9.16	35.68
32	3	43.76	tetrahedral	4,4'-azo-1,2,4-triazole, atrz	$[Ag(atrz)_{1.5}(NO_3)]_n$	257	-49.99	30,-,-	2.16	-	-	1.185	1.381	2.983	7.773	29.70
33	3	51.78	distorted octahedral	N,N-bis(1H-tetrazole-5 -yl)-amine,H_2bta	$[Co_9(bta)_{10}(Hbta)_2(H_2O)_{10}]_n$· $[22(H_2O)]_n$	300	-35.04	>40,>360,-	1.975	-	-	-	-	-	-	-

ACCEPTED MANUSCRIPT

34	3	59.85	distorted octahedral	N,N-bis(1H-tetrazole-5-yl)-amine,H_2bta	$[Co_9(bta)_{10}(Hbta)_2(H_2O)_{10}]_n$	253	-40.54	27,>360,-	1.707	859.66	-17304.47	2.317	2.658	4.537	8.657	32.18
35	3	40.08	distorted hexahedron	5-methyl tetrazole, Mtta	$[Cu_4Na(Mtta)_5(CH_3CN)]_n$	384	-71.97	36,>360,-	1.975	-	-	2.058	2.36574	4.672	7.225	24.43
36	3	45.23	distorted square pyramid	3-(1H-tetrazol-5-yl)-1H-triazole, H_2tztr	$\{[Cu(tztr)]\cdot H_2O\}_n$	325	-48.00	>40,>360, >24.75	2.316	-	-	1.1322	1.3220	3.0617	7.92	31.99
37	3	22.10	square pyramidal	3,5-dinitrobenzoic acid, 3,5-DNBA; azide , N_3	$[Cu(3,5\text{-}DNBA)(N_3)]_n$	268	-48.0	23.5,>360, -	2.030	129.28	-3464.45	-	-	-	-	-
TNT					$C_7H_5N_3O_6$	295	-73.96	15,353,0.57	1.654	-67	-	1.042	1.22	2.018	7.178	20.5
RDX					$C_3H_6N_6O_7$	210	-21.60	7.5,120,0.15	1.800	93	-	1.237	1.44	2.592	8.906	34.1
CL-20					$C_6H_6N_{12}O_{12}$	245	-10.48	4,54,-	2.035	460	-	1.338	1.554	3.162	9.385	44.9
HMX					$C_4H_8N_8O_8$	287	−21.60	7.4,-,0.2	1.950	105	-	1.130	1.320	2.574	8.900	38.39
FOX-7					$C_2H_4N_4O_4$	240	-21.62	25.2,>360, -	1.885	-133	-	-	-	-	9.09	36.6
HNB					$C_6N_6O_{12}$	240	0	1.2,-,-	1.9566	-	-	-	-	-	9.33	-
ONC					$C_8N_8O_{16}$	>200	0	-,-,-	1.979	339.13	-	-	-	-	9.8	46.7
PETN					$C_5H_8N_4O_{12}$	202	-10.1	3,60,-	1.778	-538.0	-	1.223	1.424	2.532	8.665	32.1
MF					$HgC_2N_2O_2$	165	-16.84	-,-,-	4.42	386	-	0.327	0.415	1.834	5.4	-
TATB					$C_6H_6N_6O_6$	360	-55.81	50,-,-	1.93	-154	-	0.609	0.732	1.413	8.114	31.2
tetryl					$C_7H_5N_5O_8$	129.5	-47.39	-,-,-	1.61	34	-	0.843	0.996	1.604	7.5	-

ACCEPTED MANUSCRIPT

a The nitrogen content of MOF. b Decomposition temperature. c Oxygen balance. d Impact sensitivity. e Friction sensitivity. f Electrostatic sensitivity. g From X-ray diffraction. h The standard molar enthalpy of formation. i The standard molar combustion enthalpy. j The energy of detonation (ΔE_{det})is calculated by density functional theory (DFT). k The heat of detonation ($\Delta H_{det,\ kcal\ g^{-1}}$) is estimated by using a linear correlation equation developed from known ΔH_{det} data of eleven common high explosives, ($\Delta H_{det} = 1.127\Delta E_{det} + 0.046$, r = 0.968). l The heat of detonation ($\Delta H_{det,\ kcal\ cm^{-1}}$). m Detonation velocity. n Detonation pressure. The common explosive materials: trinitrotoluene (TNT), cyclotrimethylenetrinitramine (RDX), hexanitrohexaazaisowurtzitane (CL-20), cyclotetramethylenetetranitramine (HMX), 1,1-diamino-2,2-dinitroethylene (FOX-7), hexanitrobenzene (HNB), octanitrocubane (ONC), pentaerythritol tetranitrate (PETN), mercury fulminate (MF), triaminotrinitrobenzene (TATB) and 2,4,6-trinitrophenylmethylnitramine (tetryl).

Accepted Manuscript